NASA TECHNICAL NOTE

NASA TN D-2023

DESCRIPTION AND INITIAL CALIBRATION OF THE LANGLEY HOTSHOT TUNNEL WITH SOME REAL-GAS CHARTS FOR NITROGEN

by Fred M. Smith, Edwin F. Harrison, and Pierce L. Lawing

Langley Research Center
Langley Station, Hampton, Va.

NATIONAL AERONAUTICS AND SPACE ADMINISTRATION • WASHINGTON, D. C. • DECEMBER 1963

DESCRIPTION AND INITIAL CALIBRATION OF THE LANGLEY HOTSHOT TUNNEL WITH SOME REAL-GAS CHARTS FOR NITROGEN

By Fred M. Smith, Edwin F. Harrison,
and Pierce L. Lawing

Langley Research Center
Langley Station, Hampton, Va.

NATIONAL AERONAUTICS AND SPACE ADMINISTRATION

For sale by the Office of Technical Services, Department of Commerce,
Washington, D.C. 20230 -- Price $1.50

NATIONAL AERONAUTICS AND SPACE ADMINISTRATION

TECHNICAL NOTE D-2023

DESCRIPTION AND INITIAL CALIBRATION OF THE LANGLEY HOTSHOT TUNNEL WITH SOME REAL-GAS CHARTS FOR NITROGEN

By Fred M. Smith, Edwin F. Harrison,
and Pierce L. Lawing

SUMMARY

Development and initial calibration tests of the Langley hotshot tunnel have been completed and results are presented. An arc-chamber temperature and pressure of approximately 3000° K and 10,000 pounds per square inch produced a free-stream Mach number of approximately 20 in the test section. Comparisons of various configurations and materials for the arc-chamber components are presented along with contamination measurements. Flow contamination was significantly reduced by modification of the arc-chamber configuration. Some real-gas correction factors which consider intermolecular forces and vibrational equilibrium effects for nitrogen flow in hypersonic nozzles are also presented.

INTRODUCTION

The Langley hotshot tunnel was constructed primarily to obtain force measurements, pressure distributions, and heat-transfer data for hypersonic configurations and to conduct simple flow studies over them. The tunnel was installed and shakedown tests were begun late in 1960. A number of problem areas were encountered in this initial operation; principally among them were materials for arc-chamber components (electrodes, insulators, liners, etc.), arcing at mechanical connections of the external conductors, flow contamination, and sensing instrumentation.

This report primarily presents a description of the tunnel with initial calibration and describes test and development experience with the first arc chamber, which employed opposed electrodes. The calibration indicated an approximate Mach number of 20 for arc-chamber temperatures and pressures of approximately 3000° K and 10,000 pounds per square inch with nitrogen as the flow medium. A new arc chamber utilizing end-firing coaxial electrodes has recently been installed in the Langley hotshot tunnel. A description of this chamber is presented in appendix A along with a discussion of initial test experience which demonstrated a significant decrease in contamination level. Also included in the report

(appendix B) are real-gas correction factors for nitrogen flow in hypersonic nozzles for the temperature and pressure range of this operation.

SYMBOLS

$(A/A^*)_{effective}$	ratio of effective nozzle-to-throat area (mass flow considerations)
$(A/A^*)_{geometric}$	ratio of geometric nozzle-to-throat area
$\frac{dI}{dt}$	rate of change of arc current with time
H	enthalpy
I	arc current
M	Mach number
N	consecutive number of shots for a given material or component
N_{Re}	Reynolds number per foot
p	pressure
q	dynamic pressure
R	gas constant; equal to 3.661×10^{-3} when pressure is measured in atmospheres, density in amagat units, and temperature in ^{o}K
S	entropy
t	elapsed tunnel run time
T	temperature
T_0	reference temperature, 273^{o} K
v	stream velocity
y	transverse location of pitot probe from tunnel center line
α	angle of attack of model
ρ	density, amagat units (a relative scale referred to density at 0^{o} C and 1 atmosphere of pressure; for nitrogen, 1 amagat = 0.00242 lb-sec^2/ft^4)
ϵ	energy transfer efficiency

Subscripts:

c	arc-chamber conditions before arc discharge
max	maximum
1	free-stream conditions
2	static conditions behind normal shock
i	ideal conditions
ref	reference value
t,1	arc-chamber conditions following discharge
t,2	stagnation conditions behind normal shock

An asterisk on a symbol denotes throat conditions.

DESCRIPTION AND OPERATION OF TUNNEL

A schematic diagram and a photograph of the Langley hotshot tunnel are shown in figure 1. The major components of the tunnel include a two-million-joule capacitor bank with a charging unit, an arc chamber, a 10° total-angle conical nozzle having diameters of 0.100 inch at the throat and 24 inches at the test section, a 200-cubic-foot vacuum tank, vacuum pumps, operation controls, and data-recording instrumentation.

Tunnel Operation

The operation of the Langley tunnel is similar to other hotshot facilities (refs. 1 and 2) in that a quantity of stored electrical energy is discharged across a pair of electrodes inside the arc chamber. (See fig. 2(a).) The arc gap is broken down by the exploding of a steel wire between the electrodes. The arc heats and further pressurizes the charge of test gas (nitrogen) contained within the arc chamber and results in the rupture of the diaphragm. The gas then expands through the nozzle into the vacuum chamber (both of which have been evacuated to approximately 5 microns of mercury). The run is terminated approximately 30 to 50 milliseconds later with breakdown of the flow in the test section at which time the dump valve releases the residual gas from the arc chamber. To avoid arc breakdown during the charging cycle, the electrode insulation is checked before each shot with a high-voltage, low-current source across the electrodes. After the check of the electrode insulation, and the evacuating of the nozzle, test section, and vacuum tank, the tunnel is then fired by the actuation of a 14-channel electronic programer. This programer provides millisecond control of tunnel firing, dump valve actuation, camera and recorder operation, and other instrumentation operation.

Arc Chamber

The opposed-electrode arc chamber which is shown in figure 2(a) was constructed of two concentric steel cylinders having an outside diameter of about 10 inches with a wall thickness of approximately $3\frac{1}{4}$ inches. The internal volume as shown is about 100 cubic inches but may be varied by using liners with different wall thickness. The opening to the nozzle was sealed by a poly [ethylene terephthalate] diaphragm. The other end of the chamber was sealed by a piston in the dump valve system. A second arc chamber with coaxial electrodes is described in appendix A.

External Electrical Connections

Because of the large current involved (approximately 1×10^6 amperes), numerous problems were encountered with arcing at mechanical connections of the arc-chamber external electrical conductors. (See fig. 2(b).) This arcing resulted in less energy transfer to the gas and in ultimate destruction of the conducting components. To avoid using threads as conductors and to obtain sufficient pressure between adjacent components, the configuration shown in figure 2(c) was developed. This configuration using the tapered surface connections was quite successful in eliminating the arcing.

Electrodes

The arc-chamber electrode configurations, for most tests, consisted of two main opposed electrodes and a trigger electrode perpendicular to the main electrodes. (See fig. 3(a).) A 0.026-inch-diameter steel trigger wire connected the trigger electrode to the ground electrode. The opposed electrodes functioned satisfactorily during the arc discharge except the arc column apparently impinged on the liner in the area of the ground electrode. Since the arc did not remain entirely between the electrodes and the insulators produced contamination in the test gas, a single electrode configuration shown in figure 3(b) was investigated. The single electrode arrangement was unsatisfactory because the contamination was not reduced.

Each main electrode, as shown in figure 4, consisted of an aluminum body, a tungsten tip, and an insulator with and without a cap. (Fig. 4(a) shows the electrode without a cap.) It was found during arc discharge that a cap over the face of the electrode reduced electrode erosion. A boron nitride washer with a steel band (as proposed in ref. 3) was incorporated as shown in figure 4(b). The boron nitride cracked and in some cases broke into small pieces. Therefore, after a few shots, it was discarded. Consequently, a cap made of a Teflon compound (Fluorogreen) was used in subsequent tests. (See fig. 4(c).)

Baffle Configurations

To prevent the solid contaminants from the arc chamber from entering the nozzle, various baffle configurations were installed in the arc chamber near the nozzle throat. Figure 5(a) shows a flat circular baffle plate which was supported by three screws and sleeves. During the arc discharge these support screws failed mechanically and the plate became detached. A one-piece plate with four right-angle orifices (fig. 5(b)) was next used. This baffle did not reduce the amount of contamination in the nozzle. The contaminants, which were either very small solid particles or small quantities of metallic vapor, apparently flowed along with the test gas through the baffle plate orifices into the nozzle. Based on the possibility that some of the particles could be removed by centrifugal action, a centrifuge configuration as shown in figure 5(c) was designed and constructed of various stainless steels. (A similar device was used successfully by Jim Jones of the Langley Reentry Physics Branch in shock tunnel studies (unpublished).) After tunnel firing it was apparent that some of the centrifuge components had melted and added contaminants to the flow. This device constructed of more suitable materials might perform more satisfactorily.

Heat-transfer gages indicated that the test gas initially trapped in all the baffle plates was not heated during the arc discharge and therefore the nozzle flow was cold for the first few milliseconds of the run. Based on these experimental results, no baffle configurations were used for subsequent tests.

Dump Valve

To alleviate excessive arc-chamber damage a dump valve was utilized to release residual gases (up to 95 percent of charge gas) at a predetermined time. The dump valve which consisted of a cylindrical body, a piston, a trigger, and one pressurizing and two exhaust ports (fig. 2(a)) was mounted on an extension of the upstream arc-chamber plug. A pneumatic piston held in place by a high pressure charge of gas in the dump valve cylinder blocked an exhaust passage through this plug. The pressure required in the dump valve cylinder to seal the exhaust orifice was slightly more than one-seventh of the maximum arc-chamber pressure. The residual gas in the arc chamber was released when a closely controlled trigger mechanism punctured a steel diaphragm in the dump valve pressure chamber.

The first trigger design (fig. 6(a)) employed an electrically fired powder charge to drive the plunger, but this system was found to be unreliable in giving the desired time accuracy. A pneumatically driven plunger (fig. 6(b)) which provided acceptable time accuracy was then substituted for the powder charge. The tunnel programer actuated a solenoid-operated air valve which supplied the driving force for the plunger to rupture the diaphragm.

Energy Supply

The energy for the arc was derived from a bank of 720 capacitors charged to a maximum voltage of 7500 volts. The capacitors each have an average capacitance of 95.6 microfarads and were connected in units of 10 to coaxial cables.

The capacitors were individually fused to prevent total destruction in the event of a failure. An oxygen-free copper collector sleeve and collar was provided to simultaneously terminate the coaxial cables, keep the total resistance low, and distribute the current to provide low electrical forces. (See fig. 3.)

To determine arc-discharge characteristics, a pickup coil measured dI/dt on both positive and negative electrodes. The signal was photographed on an oscilloscope. These photographed traces were transferred to the plots shown in figure 7. (The two traces were obtained from different runs.) These dI/dt traces which were integrated to show approximate current waveform indicate a nearly critically damped arc discharge of approximately 500 microseconds. The current waveform for the negative electrodes shows some irregularity. This is thought to be current lost to the arc-chamber liner, and the cause of much of the material losses from the liner. Difficulty in determining the precise location of the zero axis with respect to the dI/dt trace and the errors due to transposing of the oscilloscope trace make the current waveforms useful only for qualitative examination.

Nozzle and Test Section

The tunnel has a removable throat insert (fig. 2(a)) and a 10° total-angle conical nozzle (fig. 1) which expands to 24 inches in diameter at the test section. The diameter of the throat may be varied to provide a range of test-section Mach numbers. For all data presented herein a throat of approximately 0.100-inch diameter was employed. These throats were constructed of tungsten, although a few tests were made with copper and steel inserts, which were found to be unsatisfactory because of the change in throat geometry during the run.

The present tests utilized a 0.030-inch-thick poly [ethylene terephthalate] diaphragm with a diameter of 0.250 inch to isolate the arc chamber from the nozzle. The nozzle section of the tunnel was constructed of nickel-plated boiler plate to prevent rusting and to reduce outgassing during evacuation.

Vacuum System

The vacuum system consisted of a mechanical forepump and oil diffusion pumps capable of pumping the 200-cubic-foot nozzle and vacuum tank down to approximately 1 micron of mercury in approximately 30 minutes. A 12-inch remotely operated pneumatic valve allowed the vacuum tank to be pumped until immediately prior to firing of the tunnel to compensate for leaks and outgassing of the system.

INSTRUMENTATION

The characteristics of the tunnel imposed some rather stringent requirements on the instrumentation used to measure flow parameters. The short running time (30 to 50 milliseconds) required instrumentation with very short response times. In addition, the quantities to be measured in the stream (pressures and forces)

were very small; therefore, the instrumentation had to be sensitive enough to measure these quantities but at the same time insensitive to the solid contaminants in the flow. Force, pressure, and heat-transfer instrumentation were excited by 5-volt 20-kilocycle carrier amplifiers. The output signals from these amplifiers drove galvanometers in an oscillograph. These oscillograph traces were then reduced to a usable form.

Pressure Measuring Instrumentation

The charge pressure in the arc chamber was measured with a dial gage, and upon arc discharge the chamber stagnation pressure was measured with a high-frequency-response strain-gage transducer. Pitot pressures in the test section were measured by using variable reluctance pressure transducers. A 9-probe rake with pressure transducers connected, as shown in figure 8, was employed to survey the test-section flow. Each rake probe was provided with a contamination trap to prevent the solid contaminants in the flow from hitting and damaging the pressure transducer diaphragm. Tests were made with and without contamination traps and no appreciable changes in the measured pressures were observed.

Force Instrumentation and Models

Internal, high-frequency response (1000 cps), strain-gage balances were constructed to obtain aerodynamic forces. The high-frequency response was obtained with very stiff beams. To maintain low moments of inertia, the models were constructed of a 0.020- to 0.030-inch outer shell of magnesium or fiber glass, with enough internal material only for balance attachment. The complete model usually weighed about 50 grams.

Heat-Transfer Instrumentation

Preliminary tests were made by using 9 variable reluctance heat-transfer gages. (See ref. 1.) These gages performed satisfactorily for the particular range of heat transfer encountered in these tests with an acceptable level of electrical noise in the output signal. It was also noted that there was little change between prerun and postrun calibrations. Additional tests are being made in which thermocouple-calorimeter gages are being developed.

Velocity Measurement Instrumentation

Two measurements of stream velocity have been made which were 4 to 8 percent lower than calculated results. These successful measurements were made by observing with streak photography the propagation of the shock wave produced by an arc discharge in the stream. A similar technique was successfully used in references 4, 5, and 6.

Other methods were previously used in the Langley hotshot tunnel with less success. Several attempts were made to accelerate inserted objects to the flow

velocity but these were unsuccessful because the drag-mass ratio of the objects was too low for them to reach flow velocity. Another technique that met with less than complete success employed two sets of electrodes mounted in the tunnel. A spark was discharged across the upstream set of electrodes. The ions produced by this discharge moved downstream at flow velocity and discharged the second set of electrodes which had previously been charged to a voltage slightly less than the minimum breakdown voltage for the gas density, gap width, and electrode configuration. Unfortunately, sparks at this density were too nebulous and ill-defined for accurate time resolution; photographs of the sparks were also poorly defined.

Contamination Measurement

A rake (fig. 9(a)) was used to indicate a time-integrated contamination level in the test section. The relative (not absolute) measurements were performed by weighing the aluminum collecting disks before and after each tunnel shot. The weight differences were used to determine contamination profiles across the test core.

To determine a time resolution for the contamination flow, a small, 300-revolution-per-minute, synchronous motor was connected to drive a slotted disk in front of a piece of polished metal or plastic. (See fig. 9(b).) The time of rotation was such that a tunnel run and flow breakdown would be completed within 1 revolution.

Photographic Apparatus

A single-pass, Z-arrangement schlieren system with a continuous light source and a high-speed framing camera was used to observe the flow over bodies in the stream. Figure 10(a) shows a schlieren photograph of a hemisphere-cylinder model for a Mach number of approximately 20. A plate camera with the shutter open for the entire run was used to obtain the self-luminous photograph of the same model shown in figure 10(b).

Data-Recording Instrumentation

Most of the data have been recorded on oscillographs at speeds from 60 to 125 inches per second. An actual oscillograph record is shown in figure 11. A direct readout recorder was used in conjunction with the other oscillographs for monitoring purposes. The recording system is also adapted for incorporation of FM tape recorders.

TESTS, DATA REDUCTION, AND ACCURACY

Test Conditions

Figures 12 and 13 show the approximate potential and realized capabilities of the Langley tunnel with nitrogen flow. The theoretical properties presented in these charts were calculated from the real-gas equations developed in reference 7. A discussion of this method along with its limitations is presented in appendix B. The approximate solidification lines in figure 13 were calculated from an equation for nitrogen in reference 8. Figure 12 is a composite of four individual plots expressing arc-chamber conditions as a function of capacitance and charge density. Figure 13 was formed by the superposition of plots of Reynolds number against stagnation temperature with a given set of stagnation pressures for several Mach numbers. These data were plotted in this manner to present the relationship between the arc-chamber and the test-section conditions. Examples of the use of these charts are illustrated in the figures.

The experimental conditions obtained with nitrogen as the test gas are shown as the shaded region in figures 12 and 13. Additional tests have been made with helium as the test gas, but the results were very limited and for this reason are not included in this presentation. Most of the tests have been made for a range of arc-chamber temperatures between 2500° K and 3500° K and a range of pressures between 400 and 1000 atmospheres. These conditions indicated free-stream Mach numbers between 19 and 21. (See fig. 13.)

Data Reduction

For the present calibration tests the initial arc-chamber pressure, the arc-chamber pressure following arc discharge, and the pitot pressures in the test section were measured. With the use of these pressures all other arc-chamber and test-section thermodynamic and aerodynamic properties were calculated by using the data-reduction program from reference 7. This method of calculation is based on the assumption that uniform, equilibrium thermodynamic conditions exist in the arc chamber, although reference 4 demonstrates that the validity of this assumption is dependent upon the arc-chamber and electrode configuration. Even if the assumption should prove to be inaccurate, however, the measured arc-chamber pressure, and pitot pressure (and therefore the computed Mach number and the dynamic pressure) which are the main parameters presented herein would not be significantly affected. (See ref. 4.)

Accuracy

Uncertainties involved in the instrumentation, readability of oscillograph records, and repeatability of test conditions caused maximum probable inaccuracies in calibration data by the following amounts:

p_c, lb/sq in.	±10
$p_{t,1}$, lb/sq in.	±200

$p_{t,2}$, lb/sq in. . . . . ±0.04
M_1 . . . . . ±0.4
q_1, lb/sq in. . . . . ±0.02

DISCUSSION OF RESULTS

The preliminary calibration of the Langley hotshot tunnel for arc-chamber pressures and temperatures of approximately 10,000 pounds per square inch and 3000° K consisted of total-pressure measurements in the arc-chamber and pitot pressure measurements in the test section. A record of these measurements for a typical shot is shown along with pitot probe locations in figure 11. The reduced data obtained from this record are shown in table I. It should be noted that the probe numbers in figure 11 correspond to the nearest whole inch probe locations of table I. It may be seen from table I that probe number 5 provides the last pressure measurement within the usable test core; for this reason conditions other than the stagnation pressure are not shown for probes 6 to 9.

Pitot Pressure and Mach Number Surveys

The experimental results from a number of horizontal and vertical pitot rake surveys for a range of nozzle axial stations from 124.4 to 131.8 (fig. 1(a)) are presented in figure 14 along with corresponding Mach numbers for an elapsed run time of 10 milliseconds. In order to detect any peculiarities in the characteristics of the individual transducers, additional shots were usually made with the rake rotated 180°. This procedure was adopted to distinguish between transducer inaccuracy and flow irregularities. No distinction is made on the plots for the data obtained with the rake inverted.

Effective core diameter.- In this initial calibration the pitot rake which was 8 inches wide (see fig. 8) was used in the survey of the 22- to 24-inch test section. In order to determine the effective test core diameter, a number of shots were made at the extreme upstream and downstream stations with the rake offset from the tunnel center line well into the boundary layer. This procedure was followed for the horizontal survey only, as shown for stations 124.4 and 131.8 in figure 14(a). These data indicate an effective core diameter of approximately 8 to 10 inches with some indication that the core diameter increases between stations 124.4 and 131.8. The Mach number data outside the test core ($M > 21$) for the two extreme stations are not valid and are shown only for reference purposes.

Mach number profiles.- The variation in Mach number within the effective test core for a particular axial station is shown in figure 14 to be usually less than ±0.5 for both the horizontal and vertical surveys. The variations appear to be quite random and in no case was the variation large enough to suggest nozzle surface irregularities or other disturbances of serious consequence in the flow. Within the test core, the Mach number at all stations ranged between 19.5 and 21.

Effect of arc-chamber pressure.- Shown in figure 15 are the data of figure 14 along with data from greater elapsed run times from the same runs plotted against arc-chamber pressure. In figure 15 only the data assumed to be within the usable test core are presented. The short horizontal ticks in figure 15 represent the average of the individual pitot probe results for each shot and only these average values will be presented in subsequent plots. The range of arc-chamber pressures in figure 15 are a result of differences in energy level from shot to shot as well as several elapsed times for the same shots. No distinction is made between the two types of variations. It may be seen that the average pressure ratios are generally invariant with changes in arc-chamber pressure. The variation that occurs appears to be random, and no trends are indicated. There does appear to be a slight increase in Mach number, however, with elapsed run time and other decreases in arc-chamber pressure. For any one axial station the increase in Mach number is less than about 4 percent for a 34-percent decrease in arc-chamber pressure.

Effect of axial station.- In figure 16, the average stagnation pressure ratio and Mach number within the usable test core are presented against axial tunnel stations for an approximate arc-chamber pressure of 10,000 pounds per square inch. It was expected that as the flow moved downstream in the conical nozzle, an increase in Mach number would be experienced. Over the 8-inch nozzle length shown in figure 16, it may be seen that with the exception of stations 128 and 129.8, such a trend is indicated. At the present time the reason for the departure from this trend at the two nozzle stations is not known.

Area Ratio Comparison

In figure 17, the effective area ratio as determined from the measured arc-chamber pressure, pitot pressures, and the equation of continuity are compared with the geometric area ratio based on the geometric cross-sectional areas of the test section and the throat. For the present nozzle, the effective area ratio is shown to be about 40 to 60 percent of the geometric area ratio and compares well with the nozzle data of reference 2 also presented in figure 17.

Decay of Arc-Chamber Conditions

The rapid decay of the arc-chamber pressure during tunnel running led to an investigation in which several shots were made with a steel plate blocking the nozzle throat to prevent nozzle flow. Figure 18 presents a comparison of the results for a typical blocked throat shot with those from a normal shot. This comparison shows that for a 30-millisecond shot the losses to the arc-chamber components resulted in a 13-percent decrease in pressure whereas the nozzle flow resulted in only an additional 5-percent pressure decrease. The decrease in temperature was essentially the same for both types of shots. With increased arc-chamber energy the decay of conditions would be greater as shown in reference 5.

Representative Force Data

Some representative force and moment measurements obtained on a blunted cone utilizing a strain-gage balance are presented in figure 19. This figure shows that for a given angle of attack because of the decaying arc-chamber conditions, the dynamic pressure, normal force, and pitching moment decrease with tunnel run time; however, when these data are reduced to coefficient form, little or no change is observed with variation of run time. Additional information concerning these tests is contained in reference 9.

Tunnel Components and Materials

Arc-chamber liners.- The effective lifetimes of four types of liner materials are shown in figure 20(a) where it may be seen that the copper liner had the longest life. Damage sustained by the copper liner was caused by arc erosion, vaporization, and sputtering of the surface near the electrodes. The steel liner lost more surface material, presumably by evaporation, than the copper liner. This was also verified by higher flow contamination measurements in the test section. Nylon liners suffered very severe damage by charring and were often cracked by the shock loading. An attempt was made to flame spray a 0.025-inch-thick tungsten layer on a steel liner. The film failed mechanically from either the pressure shock loading or differential thermal expansion rates. There was some damage from arc sputtering and erosion, but apparently no evaporation damage.

Electrode insulators.- Four different types of materials were tried as electrical and thermal insulators. Figure 20(b) shows the relative lifetimes in terms of number of tunnel runs that the components remained usable. Boron nitride failed because of inability to endure the mechanical loading. Nylon and fiber glass both were damaged by charring. The fourth material, a Teflon compound, was damaged slowly in successive shots by pyrolysis, and finally failed mechanically.

Throat inserts.- In figure 20(c) it can be seen that copper and steel were unsatisfactory as materials for throat inserts since the throat diameter with these materials increased throughout the run. The tungsten inserts suffered no such increase but they did eventually fracture.

Contamination.- Figure 21 shows that the transverse distribution of mass of solid contaminants increased with increasing arc-chamber energy-input levels. It should be noted here that these results represent the contamination collected during the entire run although preliminary results with the rotating disk indicated that the contamination mass flow was uniform throughout the steady flow portion of the run and decreased rapidly at start of flow breakdown. From pitot pressure measurements it may be assumed that the mass flow of gas is constant across the test core. Therefore, it was assumed that the contamination was greater at the center of the test core (as suggested by fig. 21) because the contamination particles were originally accelerated on a path closely parallel to the tunnel longitudinal center line and the available force was insufficient to expand the heavier particles with the flow. The contamination had the following origins: electrode caps, insulating and sealing materials, material sputtered or eroded from the tungsten electrode tips and the liner, evaporation of the copper liner and steel end plates, and the steel trigger wire used to initiate the arc.

Several design features which serve to reduce flow contamination have been incorporated in a new arc chamber which is described in appendix A. Preliminary results with this arc chamber indicate an order of magnitude reduction in contamination level.

CONCLUSIONS

Preliminary development and calibration tests of the Langley hotshot tunnel for maximum arc-chamber pressures and temperatures of approximately 10,000 pounds per square inch and 3000° K have resulted in the following conclusions:

1. Pitot rake surveys indicated lateral variations in Mach number to be less than ±0.5 from the average value of 19.5 to 21 depending on the axial station.

2. Along the tunnel axis for approximately the length of one test core diameter the average Mach number variation is only slightly greater than 1.

3. From mass flow considerations, the effective test-section—throat-area ratio is approximately equal to half the geometric area ratio.

4. Blocked-throat shots indicated that temperature losses from the arc chamber are primarily a result of losses to the walls and not to the flow through the nozzle.

5. A significant decrease in contamination level has been obtained in preliminary tests with a new arc chamber with coaxial electrodes which provide for arc rotation.

Langley Research Center,
National Aeronautics and Space Administration,
Langley Station, Hampton, Va., August 7, 1963.

APPENDIX A

A NEW ARC CHAMBER WITH A MAGNETIC FIELD COIL FOR THE LANGLEY HOTSHOT TUNNEL

After approximately $1\frac{1}{2}$ years of development and operating experience with the opposed-electrode arc chamber described in this report, an arc chamber employing end-firing coaxial electrodes (fig. 22) was obtained to overcome some of the disadvantages that were apparent with the opposed-electrode configuration. Chief among these were the relatively large contamination level, the resulting low-energy transfer efficiency, the large assembly and disassembly times between shots, and the extensive maintenance required by arc-chamber components.

The new arc chamber has an internal volume of approximately 180 cubic inches (80 percent greater than the original chamber). It utilizes a single electrode assembly containing the two main electrodes and the trigger electrode and thereby reduces insulation material (a potential contamination source) as well as providing a compact electrode unit that is easily maintained and assembled. In addition, these electrodes provide an arc configuration that can be driven longitudinally and rotated. The copper liner in this configuration serves as part of the outer main electrode and thereby provides a path for longitudinal arc movement. The liner also presents a smooth surface without ports and obstructions and thereby eliminates potential erosion and contamination sources. Experimental results with this chamber indicate a measured contamination level only one-fifth as large as that for the opposed-electrode configuration. Thus, the effort to reduce contamination sources and to provide an unobstructed path for the arc resulted in a considerable reduction in contamination as well as a 10-percent increase in energy-transfer efficiency (the ratio of internal energy increase of the gas to the energy stored in the capacitors).

To insure arc rotation a 372-turn external magnetic coil (fig. 22) capable of producing a 20-kilogauss field, when cooled to liquid nitrogen temperatures, has been installed around the new chamber. The arc rotation should tend to eliminate hot spots and further reduce component erosion and burning. Insufficient experience has been obtained with the magnetic coil to evaluate its effectiveness in rotating the arc and reducing component damage, but preliminary results indicate a 50-percent reduction in measured contamination with its use. Therefore, the use of this arc chamber in conjunction with the field coil produced an order of magnitude reduction in measured contamination level when compared with the opposed-electrode arc chamber.

APPENDIX B

REAL-GAS CORRECTION FACTORS FOR NITROGEN IN HYPERSONIC NOZZLES

Presently, several hypersonic wind tunnels are using nitrogen as the flow medium at elevated stagnation temperatures and pressures where real-gas (intermolecular force) effects are important. In order to determine the true values of the thermodynamic properties of the flow, some real-gas equations have been formulated in reference 7. However, with the current use and the probable increase in the use of nitrogen in hypersonic nozzles, it appears that these real-gas effects might be presented in a more useful or convenient form. For this reason some nozzle flow properties have been calculated and are presented in figure 23 in the form of correction factors. These correction factors are the ratios of real-to-ideal gas flow parameters at the same Mach number. Shown in figure 23 are the variations in the correction factors of $p_1/p_{t,1}$, $\rho_1/\rho_{t,1}$, $T_1/T_{t,1}$, $q_1/p_{t,1}$, A_1/A^*, p_2/p_1, ρ_2/ρ_1, T_2/T_1, $p_{t,2}/p_{t,1}$, $\rho_{t,2}/\rho_{t,1}$, and $T_{t,2}/T_{t,1}$ with stagnation pressures ranging from 500 to 2500 atmospheres and for stagnation temperatures of 2500° K, 3000° K, 3500° K, and 4000° K.

The real-gas data in the correction factors were determined from equations (ref. 7) which include intermolecular force (so-called Van der Waals' effects) and vibrational equilibrium effects. Vibrational nonequilibrium effects (ref. 10) are not considered here but for some conditions may be important. These equations were used for stagnation temperatures ranging from 2500° K to 4000° K which includes 500° K below the reference data limits. However, the results at 2500° K show good agreement with the real-gas data in reference 11. Because of the lack of data, no comparison was made for the 4000° K results. It was assumed for the real-gas data that the inviscid core of the gas through the nozzle was one-dimensional, adiabatic, equilibrium nitrogen flow. The ideal-gas properties were taken from reference 12. All flow parameters presented herein are essentially invariant with Mach numbers above 10.

In the calibration of most hypersonic nozzles ($M \geqq 10$) the stagnation reservoir pressure and temperature and pitot pressure behind the normal shock in the nozzle are usually measured. With these measured quantities and the charts in figure 23, the Mach number and other real-gas flow parameters may be determined in the following manner: assume $p_{t,1} = 800$ atmospheres, $T_{t,1} = 3000°$ K, and $p_{t,2} = 0.068$ atmosphere and from figure 23(i) for these conditions $\dfrac{(p_{t,2}/p_{t,1})}{(p_{t,2}/p_{t,1})_i} = 0.658$; therefore, the value of $(p_{t,2}/p_{t,1})_i$ is 0.1292×10^{-3}. With this ideal stagnation pressure ratio, a real-gas, free-stream Mach number of 19.28 can be obtained from the tables of reference 12. In addition, all other corresponding ideal-gas flow parameters can be found for this Mach number $(M_1 = 19.28)$ in these tables, for example, $(T_1/T_{t,1})_i = 0.01327$. Then the

values of all other real-gas flow variables can be easily determined from the correction factors in figure 23 and the above ideal-gas flow parameters. For example, substitution of these values in the expression

$$\frac{T_1/T_{t,1}}{(T_1/T_{t,1})_i} = 1.1877$$

yields

$$T_1 = 47.3^\circ \text{ K}$$

From figure 23 it can be seen there is a wide range of variation of the real-gas effects on various flow parameters: up to 200 percent for the nozzle area ratio (fig. 23(e)) and only 4 percent for the static pressure ratio (fig. 23(f)) at a stagnation temperature of 4000° K. Most correction factors are strongly dependent on the stagnation temperature.

Figure 24 shows the approximate maximum Mach number attainable without condensation (solidification) by the isentropic expansion from various combinations of stagnation temperature and pressure for equilibrium conditions. These curves were obtained from the solidification equation given in reference 8 and the tabulated values in reference 13 for nitrogen. The values presented in figure 24 are to be considered simply as reasonable estimates.

REFERENCES

1. Perry, R. W., and MacDermott, W. N.: Development of the Spark-Heated, Hypervelocity, Blowdown Tunnel-Hotshot. AEDC-TR-58-6, ASTIA Doc. No. AD-157138, Arnold Eng. Dev. Center, June 1958.

2. Lukasiewicz, J., Harris, W. G., Jackson, R., Van der Bliek, J. A., and Miller, R. M.: Development of Capacitance and Inductance Driven Hotshot Tunnels. AEDC-TN-60-222 (Contract No. AF 40(600)-800 S/A 11(60-110)), Arnold Eng. Dev. Center, Jan. 1961.

3. Kyser, James B.: Development of a Hotshot Arc Chamber for Long Component Life and Low Gas Contamination. Proc. Nat. Symposium on Hypervelocity Techniques, Inst. Aero. Sci., Oct. 1960, pp. 98-104.

4. Karamcheti, Krishnamurty, Vali, Walter, Kyser, James B., and Rasmussen, Maurice L.: Measurements of Pressure and Speed of Flow in a Spark-Heated Hypersonic Wind Tunnel. AEDC-TDR-62-218 (ASTIA Doc. No. 288668), Arnold Eng. Dev. Center, Nov. 1962.

5. Lukasiewicz, J., Jackson, R., and Whitfield, J. D.: Status of Development of Hotshot Tunnels at the AEDC. Presented at meeting on High Temperature Aspects of Hypersonic Flow (Rhode-Saint-Genese, Belgium), AGARD, Apr. 1962.

6. Hurdle, C. V.: The Determination of Stagnation Temperature From Flow Velocity Measurements Using a Spark Disturbance Method in a Hypersonic Gun Tunnel. Memo (B) 60/62, Royal Armament Res. and Dev. Establishment, Dec. 1962.

7. Grabau, Martin, Humphrey, Richard L., and Little, Wanda J.: Determination of Test-Section, After-Shock, and Stagnation Conditions in Hotshot Tunnels Using Real Nitrogen at Temperatures From 3000° to 4000°K. AEDC-TN-61-82 (Contract No. AF 40(600)-800 S/A 24(61-73)), Arnold Eng. Dev. Center, July 1961.

8. Hilsenrath, Joseph, Beckett, Charles W., et al.: Tables of Thermal Properties of Gases. NBS Cir. 564, U.S. Dept. Commerce, 1955.

9. Harrison, Edwin F.: Static Stability Tests in the Langley 24-Inch Hypersonic Arc Tunnel on a Blunted Cone at a Mach Number of 20. NASA TN D-1508, 1962.

10. Erickson, Wayne D.: Vibrational-Nonequilibrium Flow of Nitrogen in Hypersonic Nozzles. NASA TN D-1810, 1963.

11. Clark, Frank L., and Johnson, Charles B.: Real-Gas Hypersonic-Nozzle Flow Parameters for Nitrogen in Thermodynamic Equilibrium. NASA TN D-2019, 1963.

12. Ames Research Staff: Equations, Tables, and Charts for Compressible Flow. NACA Rep. 1135, 1953. (Supersedes NACA TN 1428.)

13. Din, F., ed.: Thermodynamic Functions of Gases. Vol. 3 - Methane, Nitrogen, Ethane. Butterworths (London), 1961.

TABLE I.- RESULTS OF A CALIBRATION SHOT WITH NITROGEN AS THE FLOW MEDIUM

[See fig. 11 for pitot rake location in test section]

Arc chamber					Test section													
Stagnation conditions					Probe location	Static conditions ahead of normal shock								Stagnation conditions behind normal shock				
$p_{t,1}$, lb/sq in.	$\rho_{t,1}$, amagat	$T_{t,1}$, °K	$\frac{H_{t,1}}{RT_0}$	$\frac{S_{t,1}}{R}$	y, in. from center line	p_1, lb/sq in.	ρ_1, amagat	T_1, °K	v_1, ft/sec	M_1	q_1, lb/sq in.	N_{Re}, per ft	A/A^*	$p_{t,2}$, lb/sq in.	$\rho_{t,2}$, amagat	$T_{t,2}$, °K	$\frac{H_{t,2}}{RT_0}$	$\frac{S_{t,2}}{R}$
t = 0 msec																		
12,200	62.1	3,350	51.6	25.9	----	----------	----------	--	-----	----	----	----------	----------	----	----------	-----	----	----
t = 10 msec																		
11,200	60.8	3,150	48.2	25.7	1.2	0.17×10^{-2}	0.65×10^{-3}	48	9,100	19.6	0.45	0.22×10^{6}	0.23×10^{5}	0.84	0.49×10^{-2}	3,200	48.2	35.3
11,200	60.8	3,150	48.2	25.7	2.2	.17	.66	48	9,100	19.5	.46	.23	.23	.86	.50	3,200	48.2	35.2
11,200	60.8	3,150	48.2	25.7	3.2	.18	.67	48	9,100	19.5	.46	.23	.23	.87	.51	3,200	48.2	35.2
11,200	60.8	3,150	48.2	25.7	4.2	.16	.64	48	9,100	19.7	.44	.22	.27	.83	.48	3,200	48.2	35.3
11,200	60.8	3,150	48.2	25.7	5.2	.16	.64	47	9,100	19.7	.44	.22	.24	.83	.48	3,200	48.2	35.3
11,200	60.8	3,150	48.2	25.7	[a]6.2	----------	----------	--	-----	----	----	----------	----------	.68	----------	-----	----	----
11,200	60.8	3,150	48.2	25.7	7.2	----------	----------	--	-----	----	----	----------	----------	.47	----------	-----	----	----
11,200	60.8	3,150	48.2	25.7	8.2	----------	----------	--	-----	----	----	----------	----------	.38	----------	-----	----	----
11,200	60.8	3,150	48.2	25.7	9.2	----------	----------	--	-----	----	----	----------	----------	.09	----------	-----	----	----
t = 20 msec																		
10,500	59.7	3,000	45.9	25.6	1.2	0.16×10^{-2}	0.65×10^{-3}	45	8,800	19.7	0.43	0.23×10^{6}	0.23×10^{5}	0.79	0.48×10^{-2}	3,000	45.9	35.1
10,500	59.7	3,000	45.9	25.6	2.2	.15	.63	44	8,800	19.8	.41	.23	.24	.77	.47	3,000	45.9	35.1
10,500	59.7	3,000	45.9	25.6	3.2	.16	.65	45	8,800	19.7	.43	.23	.23	.80	.49	3,000	45.9	35.1
10,500	59.7	3,000	45.9	25.6	4.2	.15	.63	44	8,800	19.9	.41	.23	.24	.77	.47	3,000	45.9	35.1
10,500	59.7	3,000	45.9	25.6	5.2	.15	.62	44	8,800	19.9	.41	.23	.24	.76	.46	3,000	45.9	35.1
10,500	59.7	3,000	45.9	25.6	[a]6.2	----------	----------	--	-----	----	----	----------	----------	.60	----------	-----	----	----
10,500	59.7	3,000	45.9	25.6	7.2	----------	----------	--	-----	----	----	----------	----------	.46	----------	-----	----	----
10,500	59.7	3,000	45.9	25.6	8.2	----------	----------	--	-----	----	----	----------	----------	.23	----------	-----	----	----
10,500	59.7	3,000	45.9	25.6	9.2	----------	----------	--	-----	----	----	----------	----------	.05	----------	-----	----	----
t = 30 msec																		
9,800	58.6	2,900	43.6	25.4	1.2	0.15×10^{-2}	0.65×10^{-3}	43	8,600	19.8	0.41	0.24×10^{6}	0.23×10^{5}	0.76	0.49×10^{-2}	2,900	43.6	34.9
9,800	58.6	2,900	43.6	25.4	2.2	.15	.64	43	8,600	19.8	.40	.24	.23	.75	.48	2,900	43.6	35.0
9,800	58.6	2,900	43.6	25.4	3.2	.15	.64	42	8,600	19.8	.40	.24	.23	.75	.47	2,900	43.6	35.0
9,800	58.6	2,900	43.6	25.4	4.2	.14	.62	42	8,600	20.0	.39	.24	.24	.72	.46	2,900	43.6	35.0
9,800	58.6	2,900	43.6	25.4	5.2	.14	.62	42	8,600	20.0	.39	.24	.24	.73	.47	2,900	43.6	35.0
9,800	58.6	2,900	43.6	25.4	[a]6.2	----------	----------	--	-----	----	----	----------	----------	.55	----------	-----	----	----
9,800	58.6	2,900	43.6	25.4	7.2	----------	----------	--	-----	----	----	----------	----------	.46	----------	-----	----	----
9,800	58.6	2,900	43.6	25.4	8.2	----------	----------	--	-----	----	----	----------	----------	.22	----------	-----	----	----
9,800	58.6	2,900	43.6	25.4	9.2	----------	----------	--	-----	----	----	----------	----------	.05	----------	-----	----	----

[a]Indicates the location of the first pitot probe beyond the usable test core.

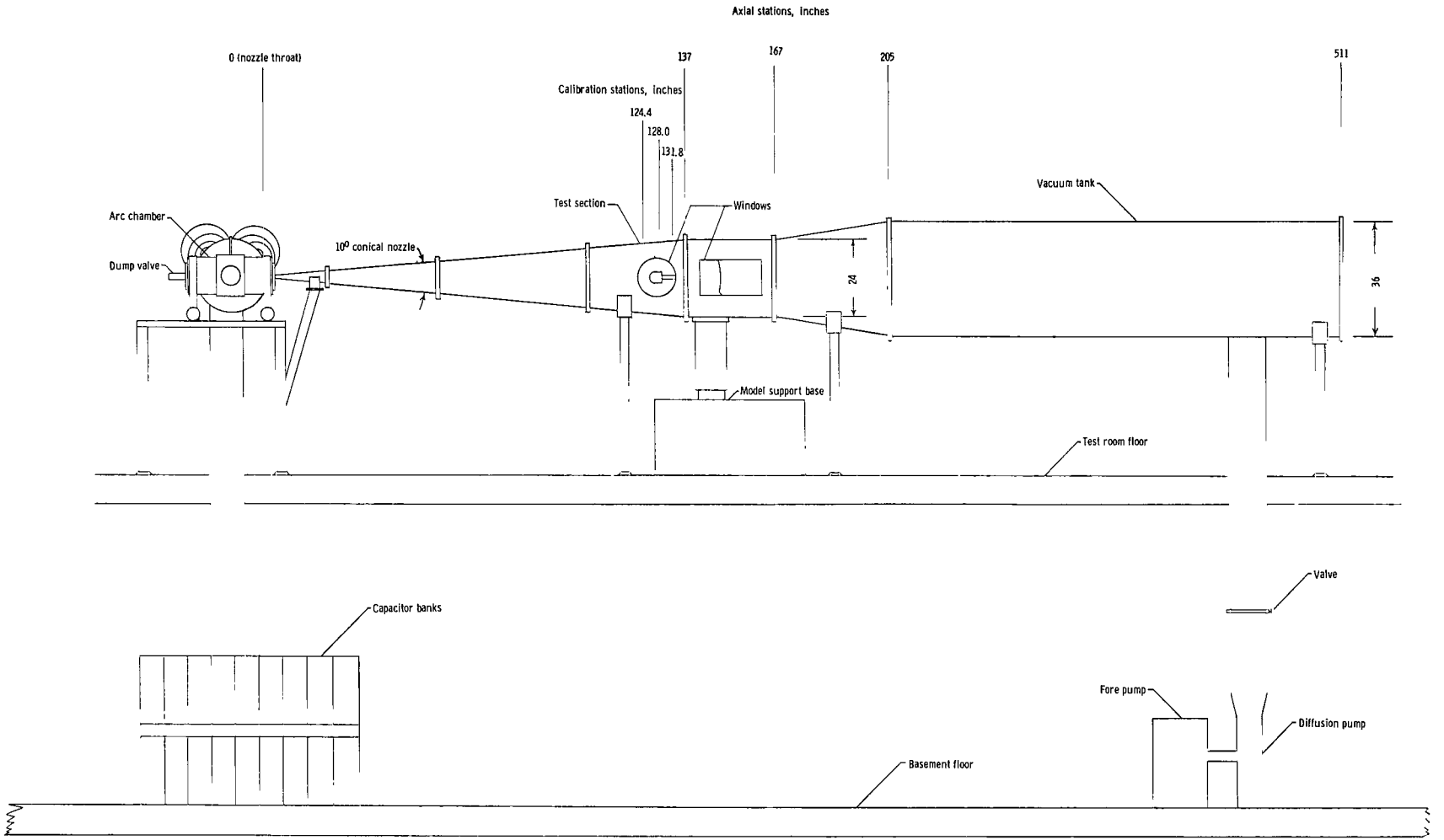

(a) Elevation sketch of the tunnel and major components. All dimensions are in inches.

Figure 1.- Langley hotshot tunnel.

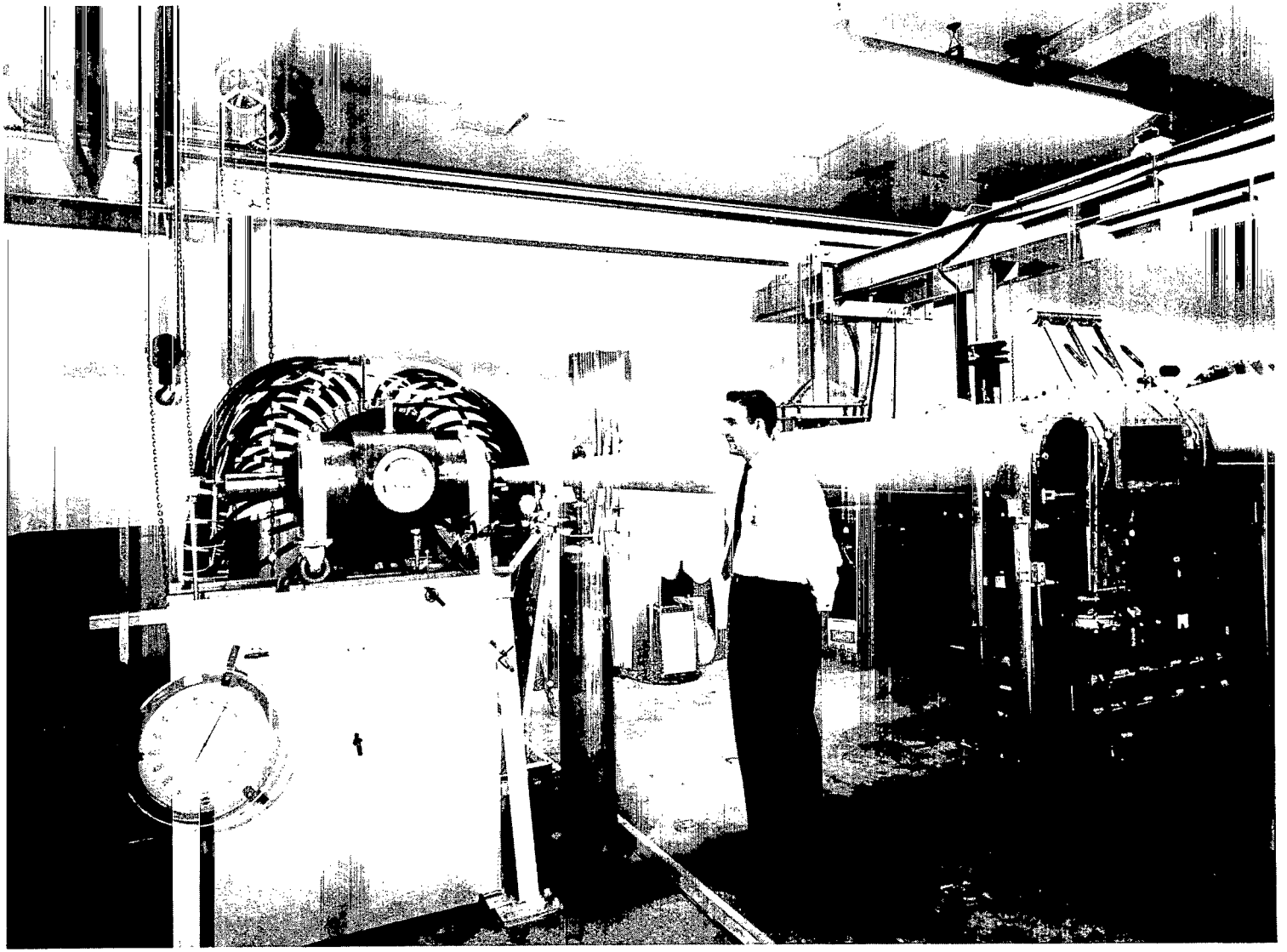

(b) Photograph of the tunnel showing the arc chamber, nozzle, and test section. L-60-8526

Figure 1.- Concluded.

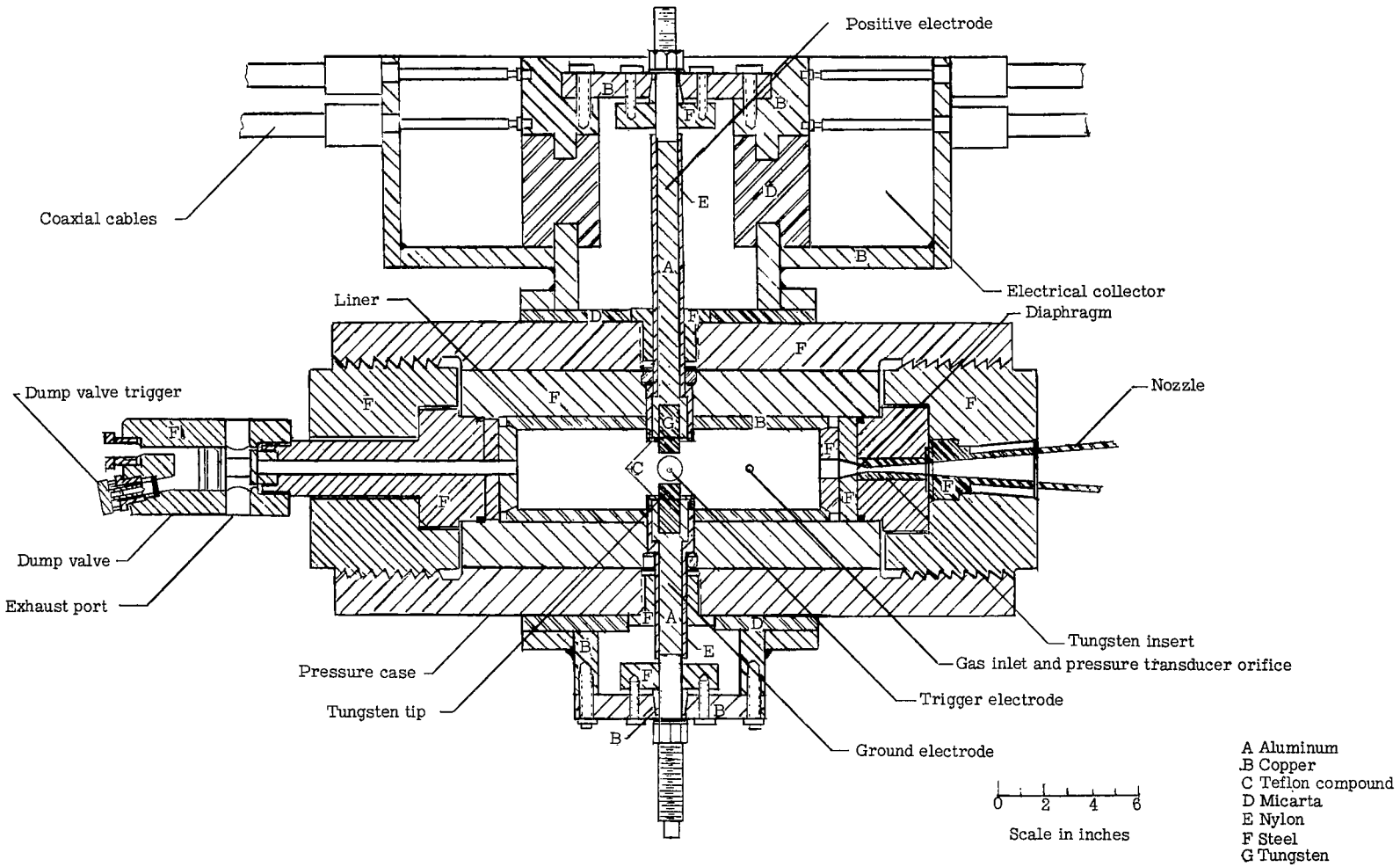

(a) Section view of the arc chamber and electrical collector and electrodes.

Figure 2.- Opposed-electrode arc chamber for the Langley hotshot tunnel.

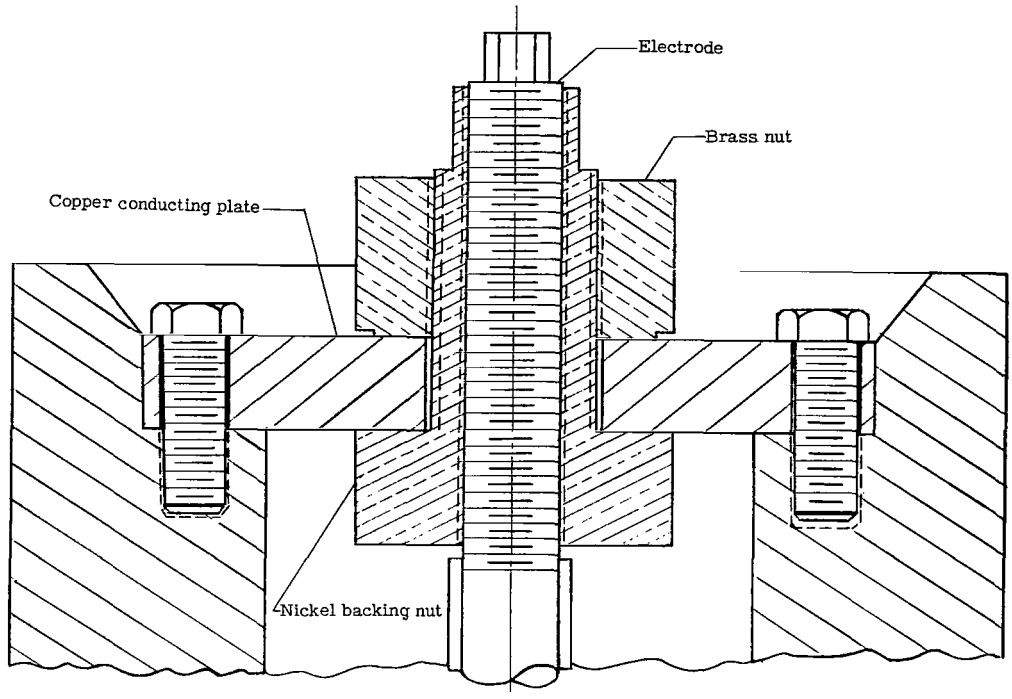

(b) Original external electrical connections for the arc chamber.

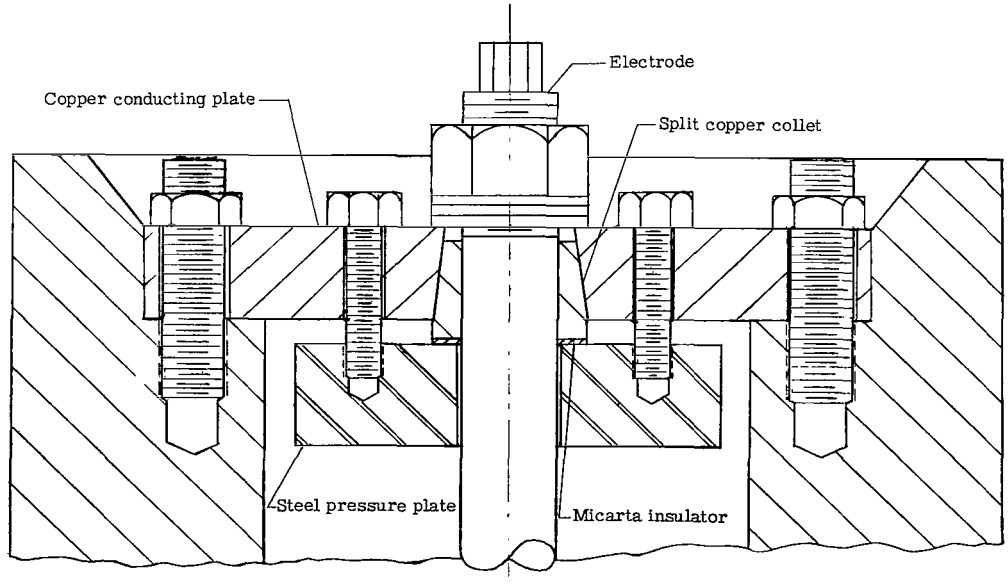

(c) Modified external electrical connections for the arc chamber.

Figure 2.- Concluded.

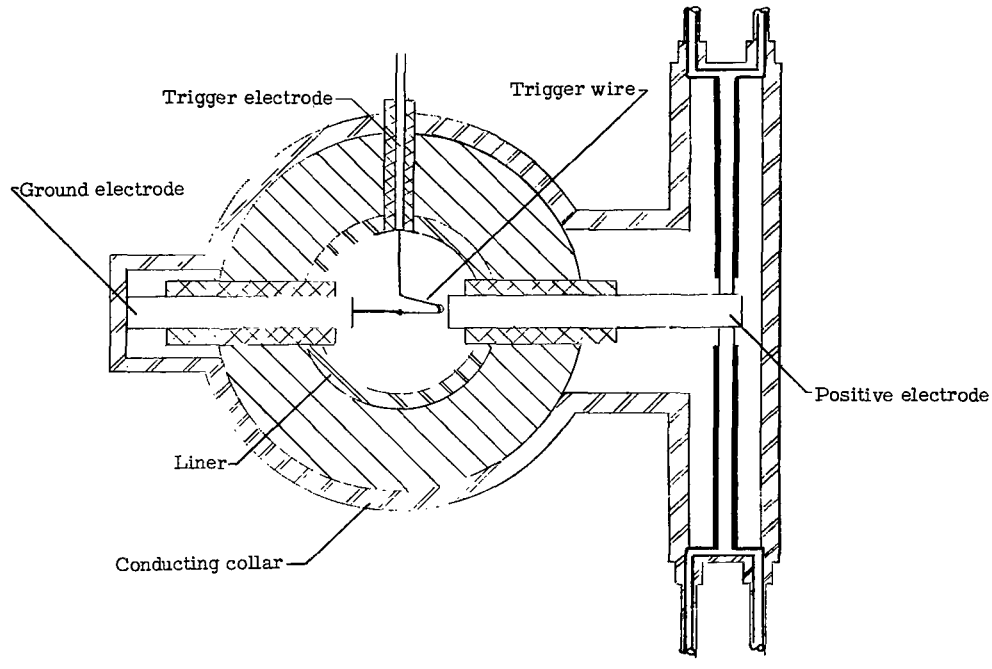

(a) Opposed-electrode configuration.

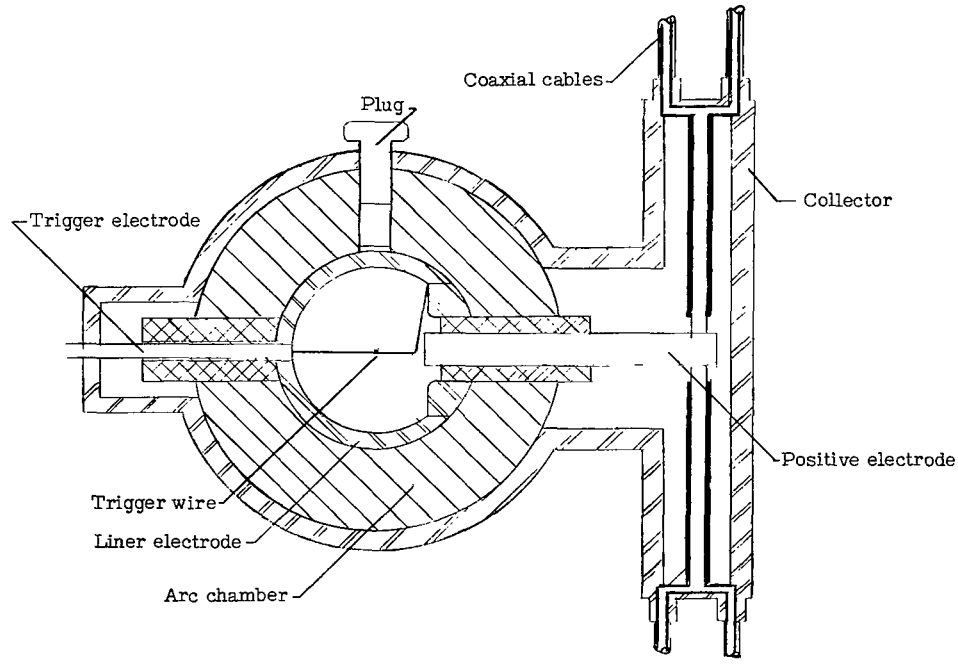

(b) Single-electrode configuration.

Figure 3.- Electrode arrangements used in the arc chamber.

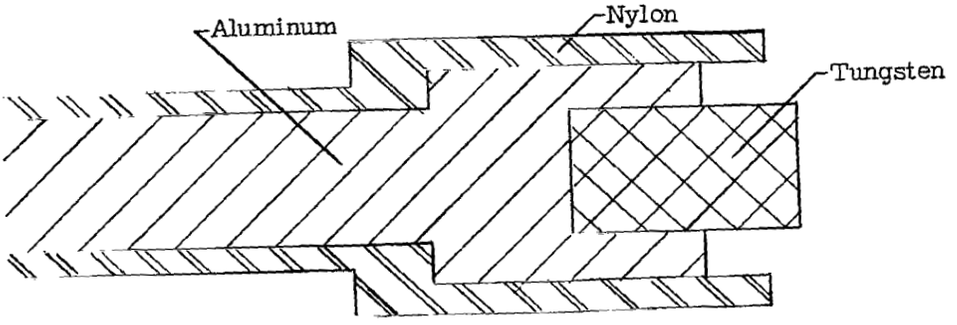

(a) Nylon insulator.

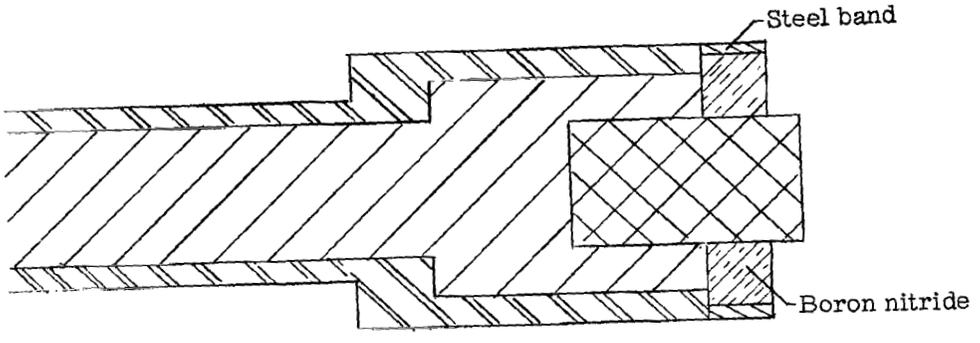

(b) Nylon insulator with boron nitride cap.

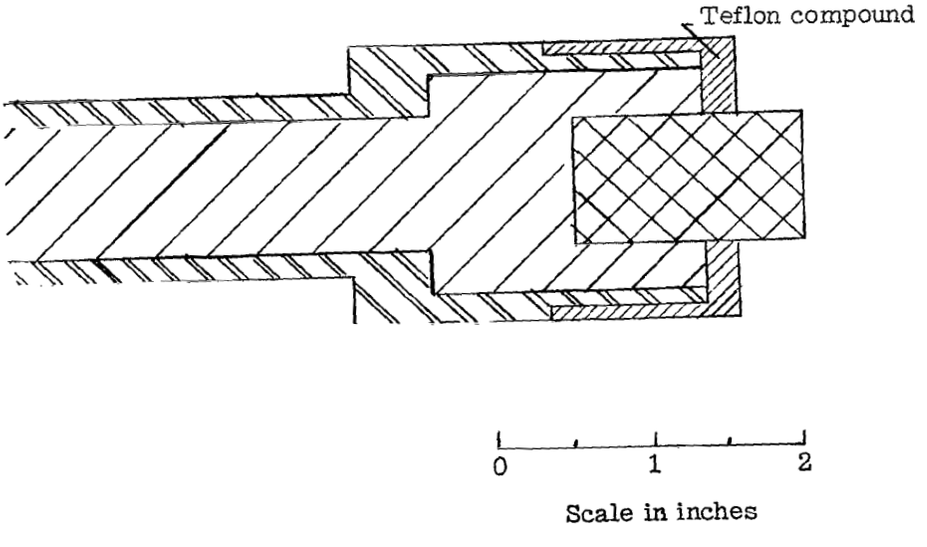

(c) Nylon insulator with cap.

Figure 4.- Section view of three electrode insulator configurations.

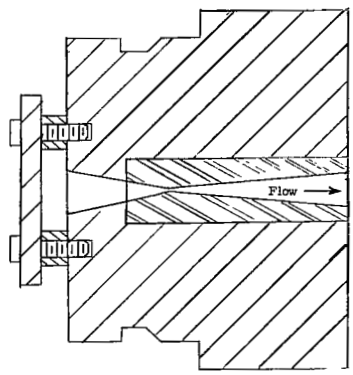

(a) Flat plate.

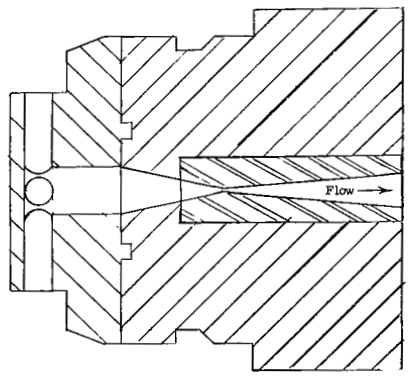

(b) Four-orifice plate.

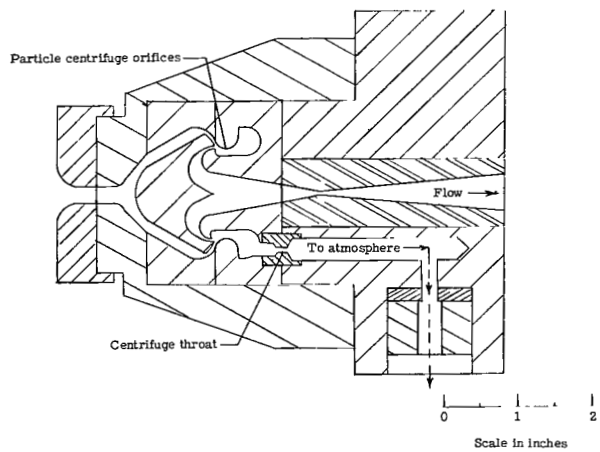

(c) Centrifuge configuration.

Figure 5.- Section view of three throat baffle configurations.

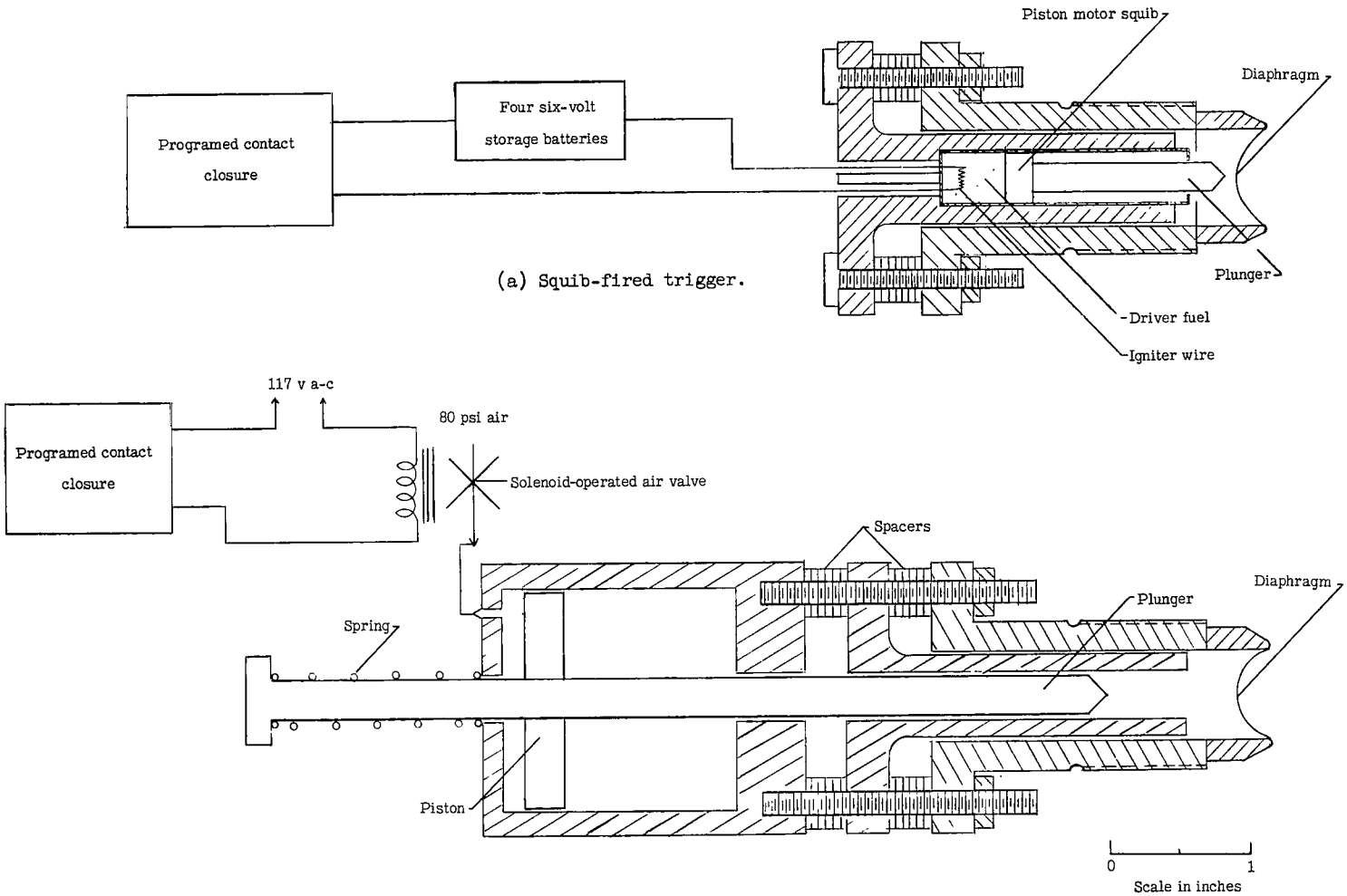

(a) Squib-fired trigger.

(b) Pneumatic valve trigger.

Figure 6.- Sketches of two dump valve triggers.

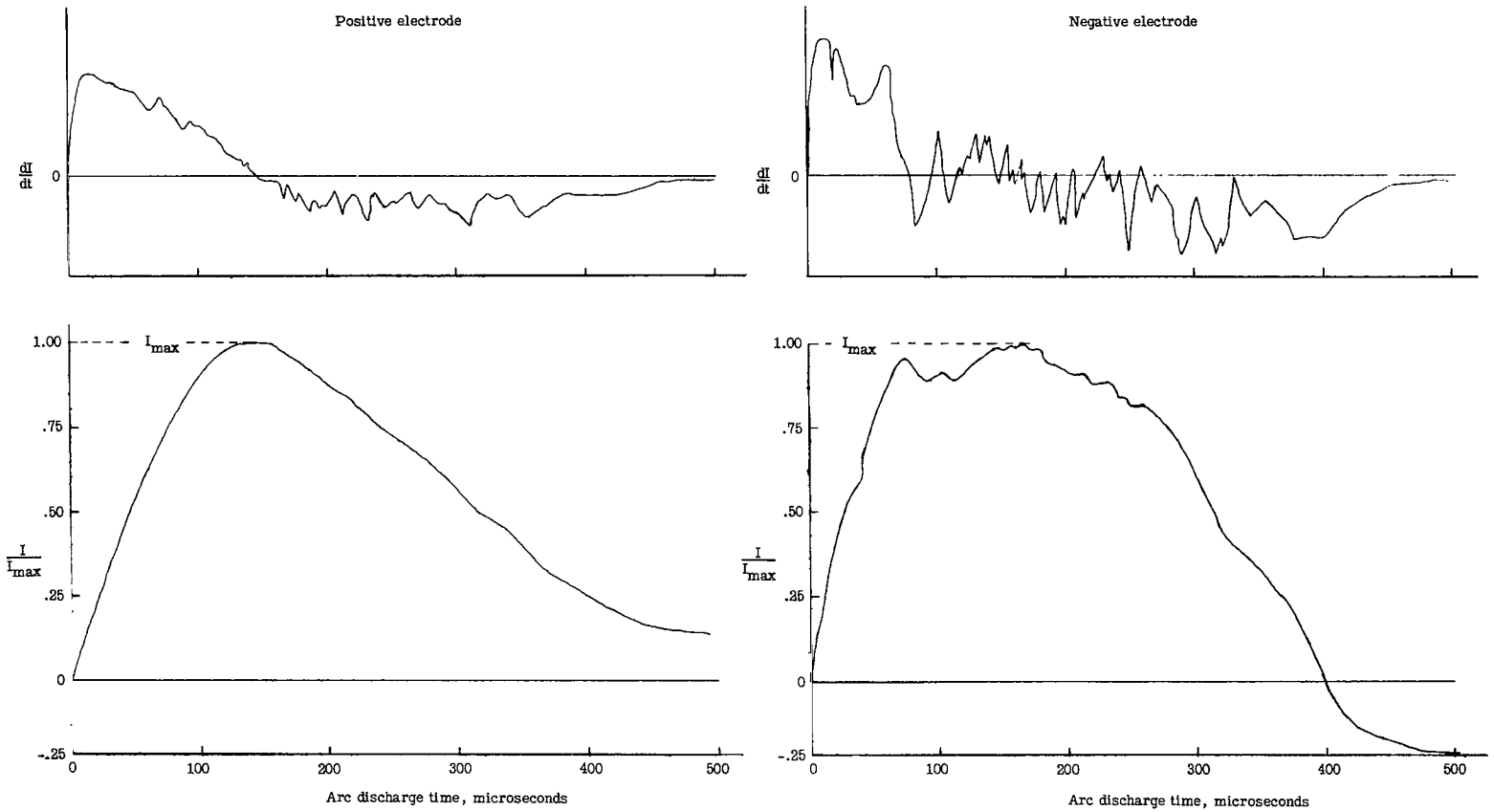

Figure 7.- Typical arc-discharge wave forms for the Langley hotshot tunnel.

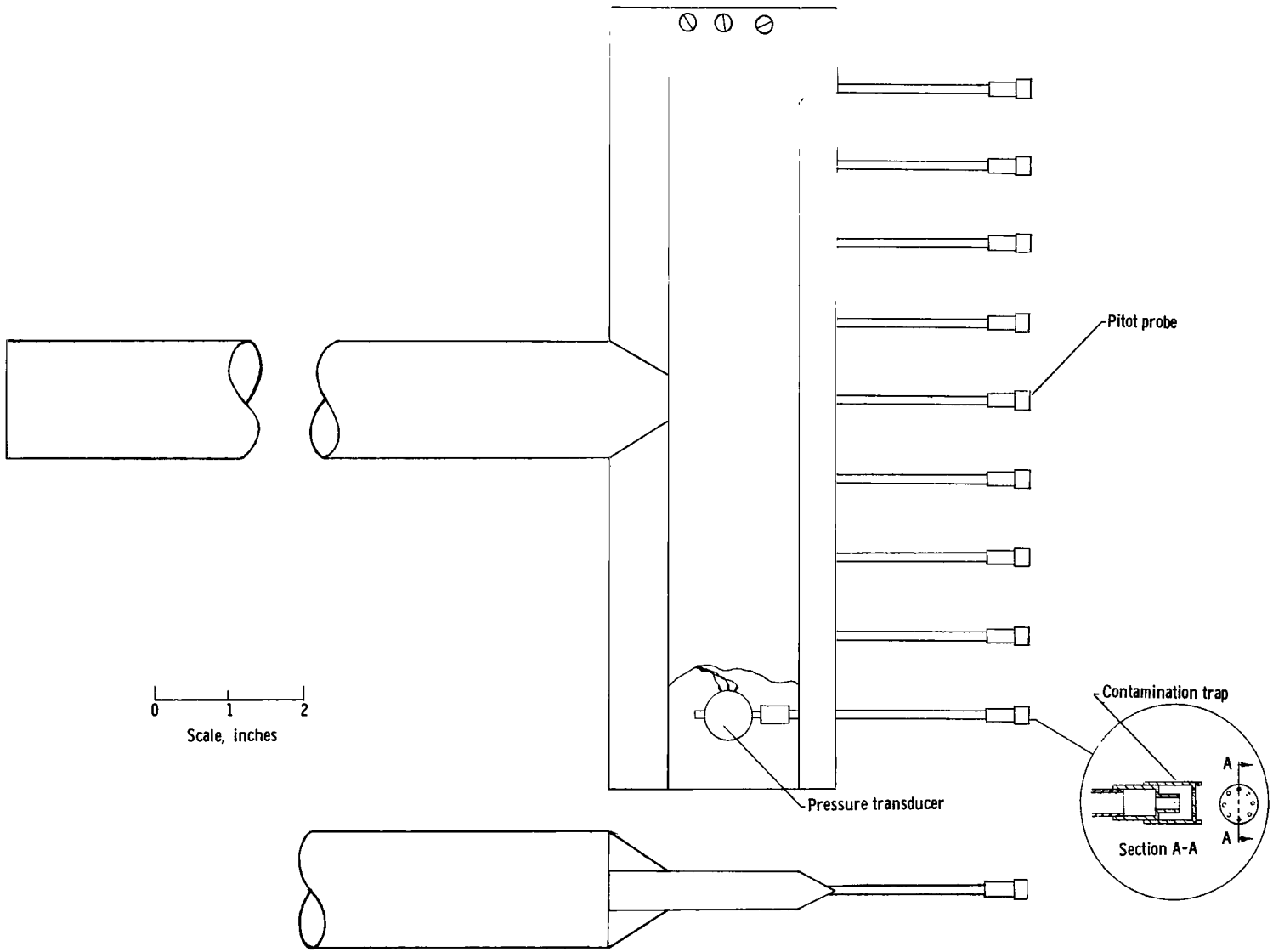

Figure 8.- Pitot pressure survey rake.

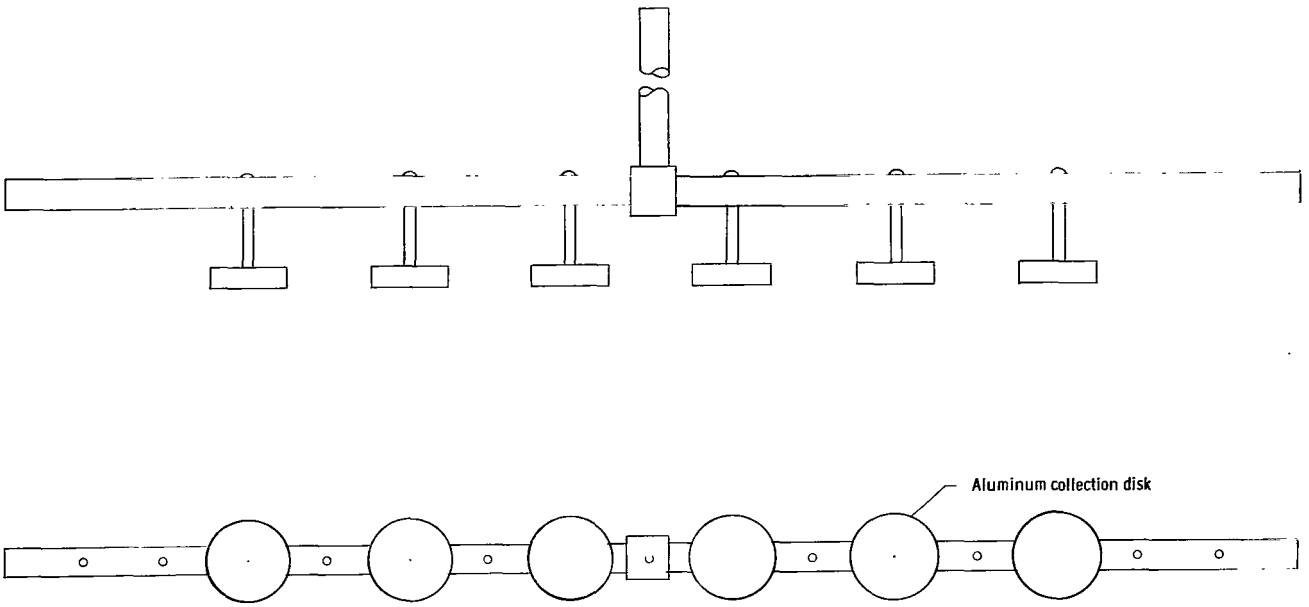

(a) Disk rake collector.

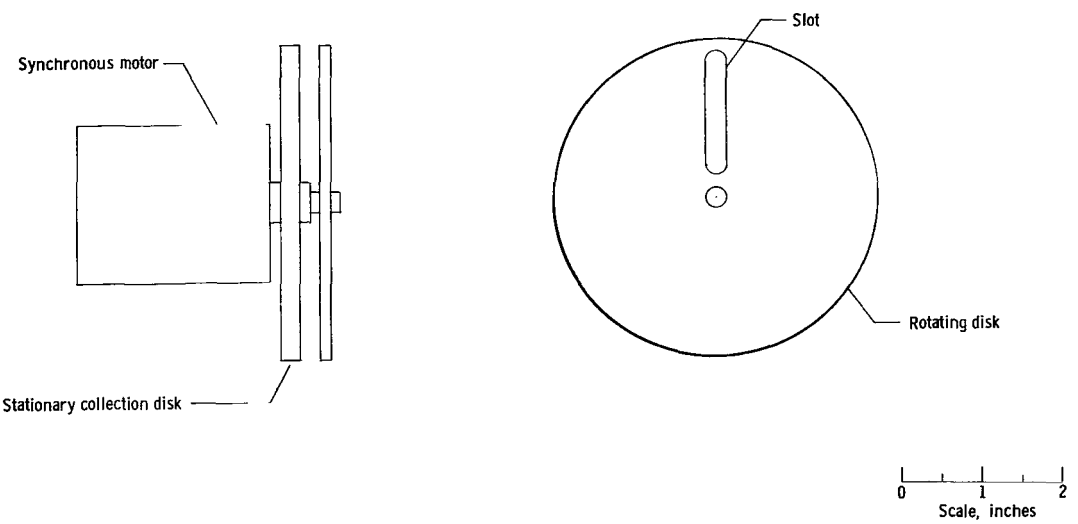

(b) Rotating disk collector.

Figure 9.- Devices used in the Langley hotshot tunnel for the collection of solid contaminants.

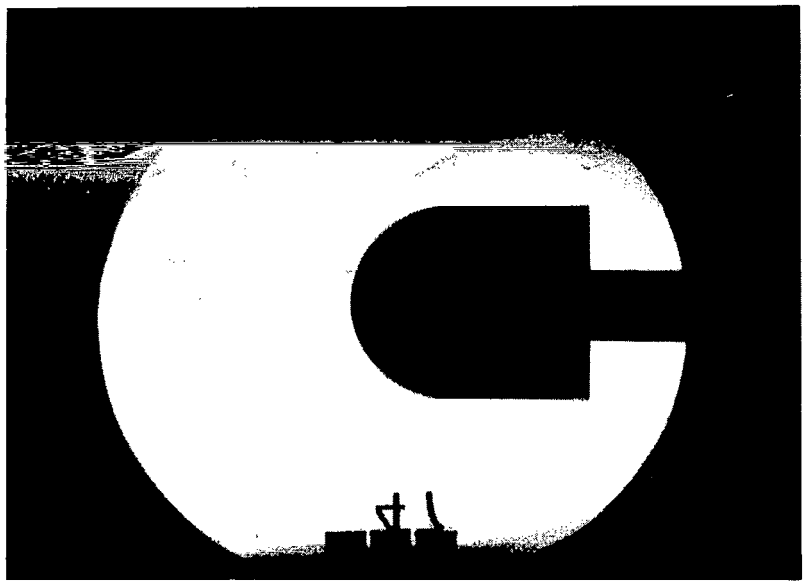

(a) Schlieren photograph.

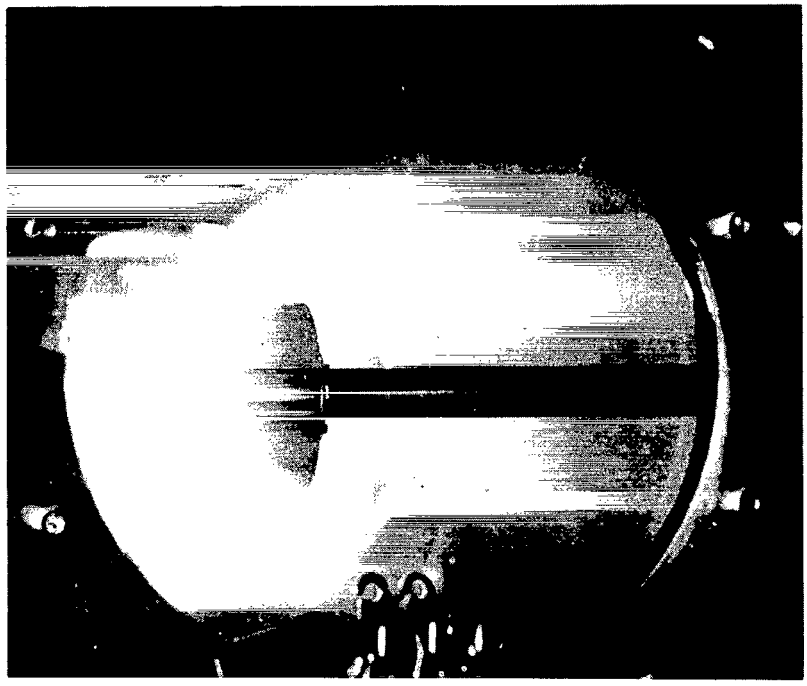

(b) Self-luminous photograph. L-63-4734

Figure 10.- Photograph of a hemisphere-cylinder model in the Langley hotshot tunnel at M = 20.

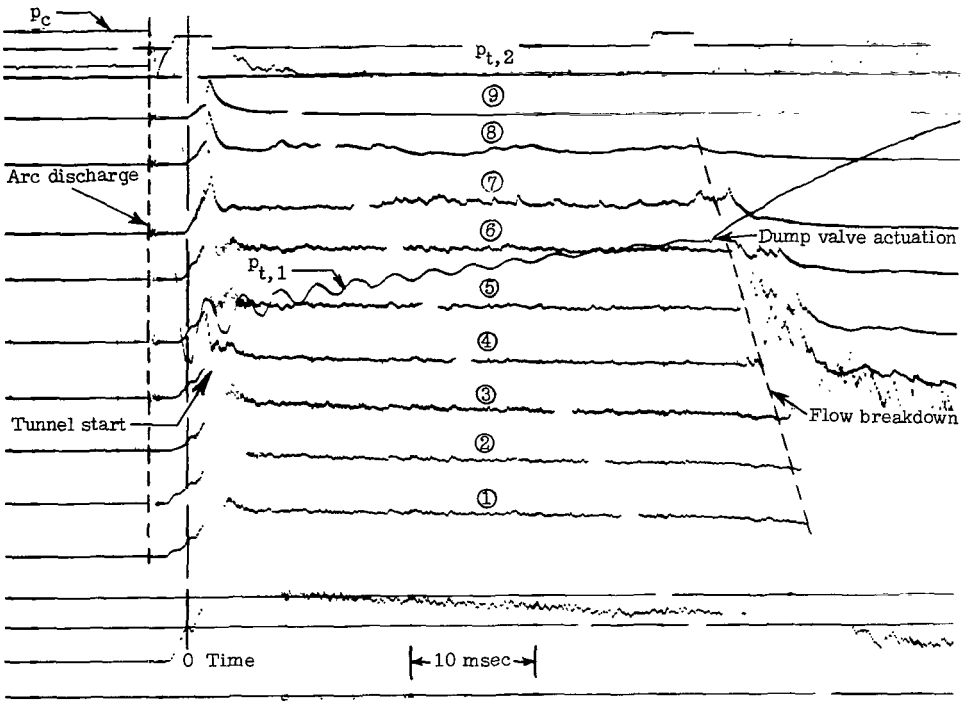

(a) Oscillograph pressure record.

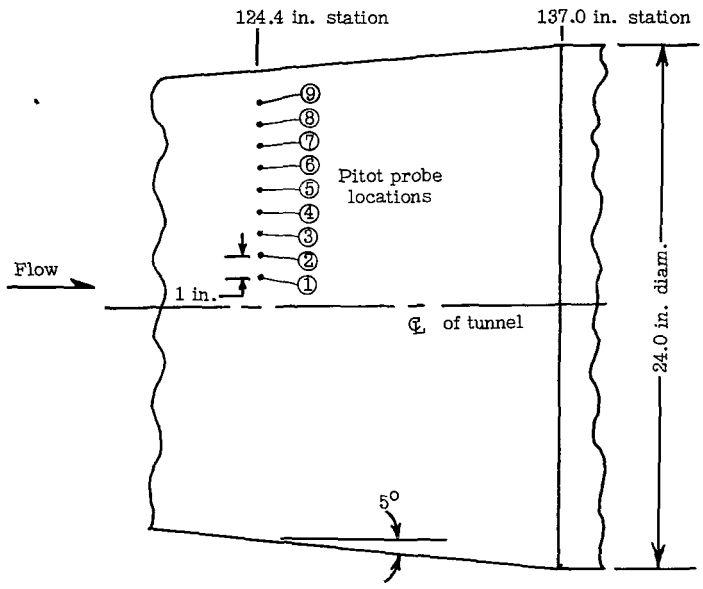

(b) Test section viewed from above.

Figure 11.- A typical oscillograph pressure record and a diagram showing location of pitot probes in the test section.

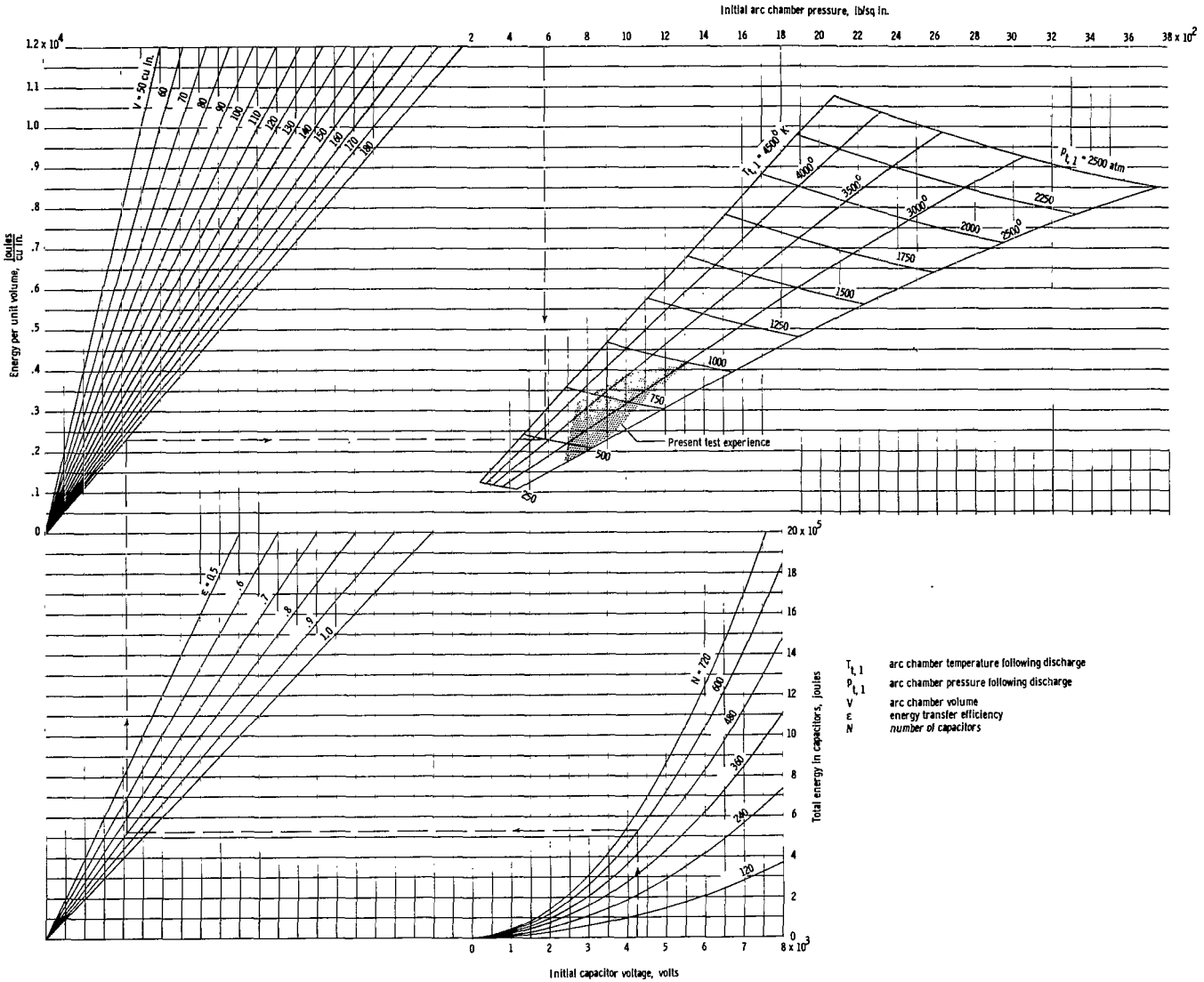

Figure 12.- Potential arc-chamber conditions for the Langley hotshot tunnel as a function of capacitance and charge density for nitrogen. (Dashed lines illustrate use of this chart: Initial capacitor voltage = 4250 volts; N = 600; ϵ = 0.80; V = 180 cu in.; $T_{t,1}$ = 3600° K; $P_{t,1}$ = 500 atm; and initial arc-chamber pressure = 580 lb/sq in.) Each capacitor has an average capacitance of 96.5 μfarads.

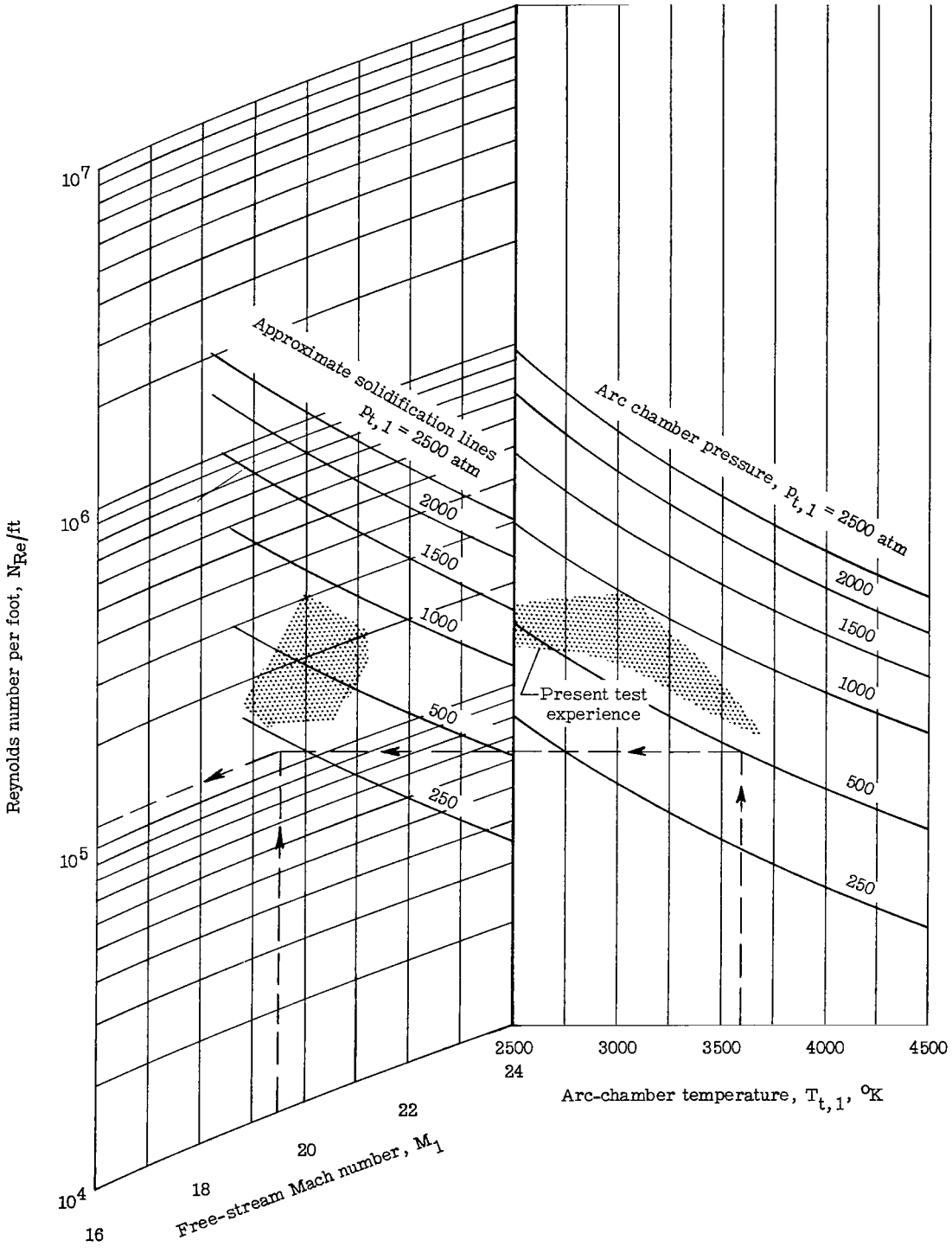

Figure 13.- Potential test-section conditions as a function of arc-chamber conditions in the Langley hotshot tunnel for nitrogen. (Dashed lines illustrate use of this chart. For $T_{t,1}$ = 3600° K, $p_{t,1}$ = 500 atm, and M_1 = 19.5, N_{Re}/ft = 1.15 × 10^5.)

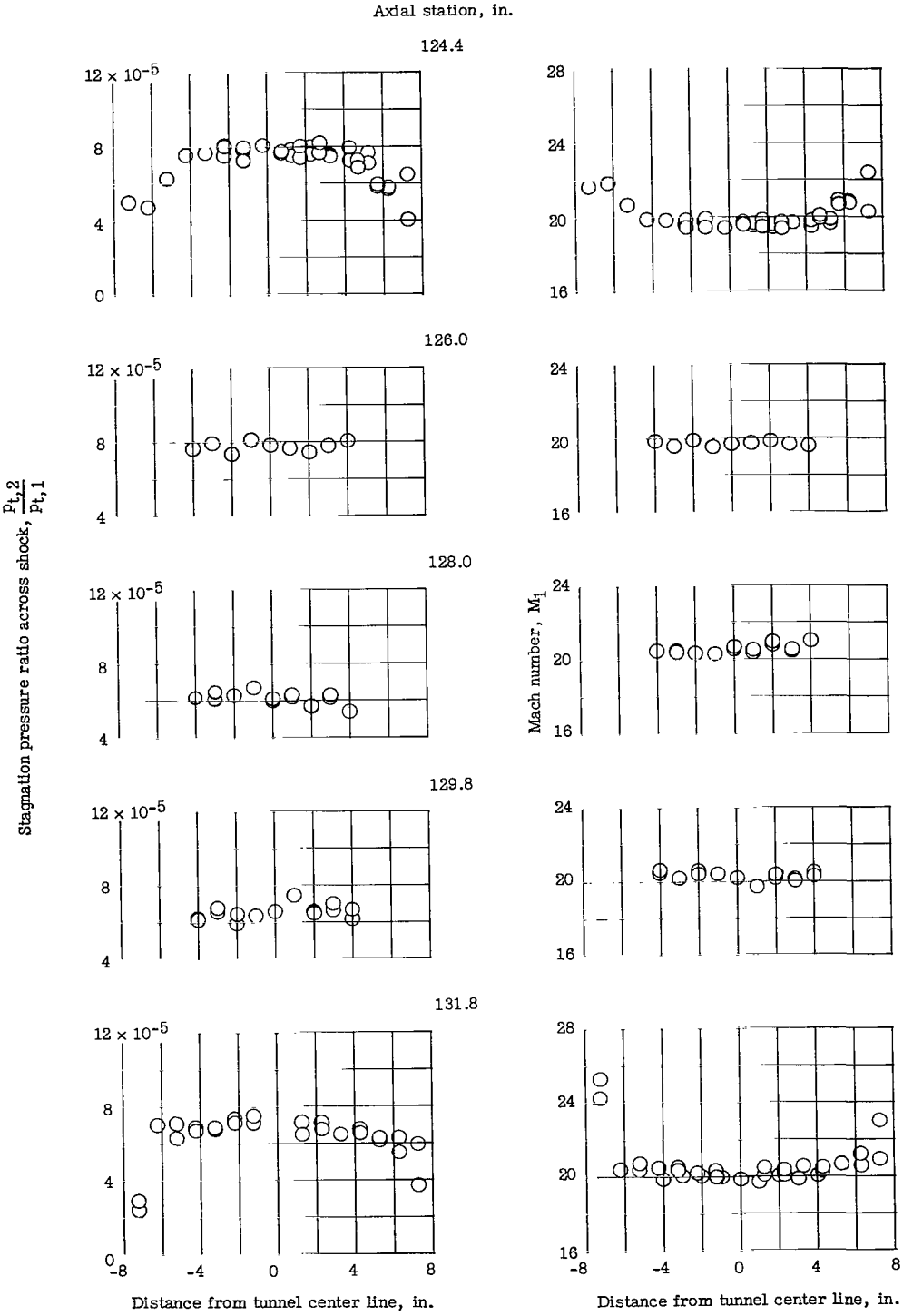

(a) Horizontal survey.

Figure 14.- Stagnation pressure ratio and Mach number profiles in the test section of the Langley hotshot tunnel. ($p_{t,1}$ = 7600 to 11,600 lb/sq in.; $T_{t,1}$ = 2250° to 3250° K; run time = 10 msec.)

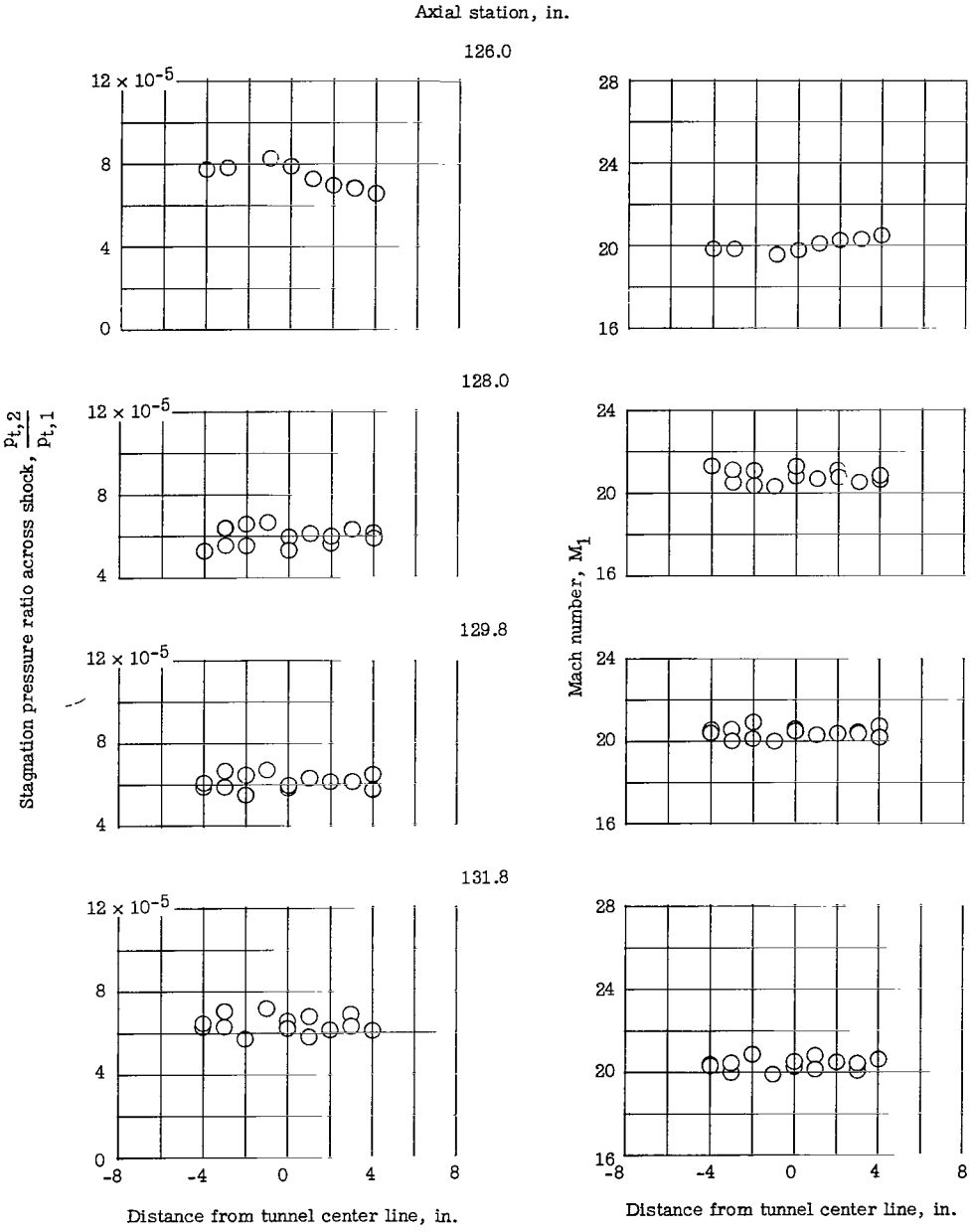

(b) Vertical survey.

Figure 14.- Concluded.

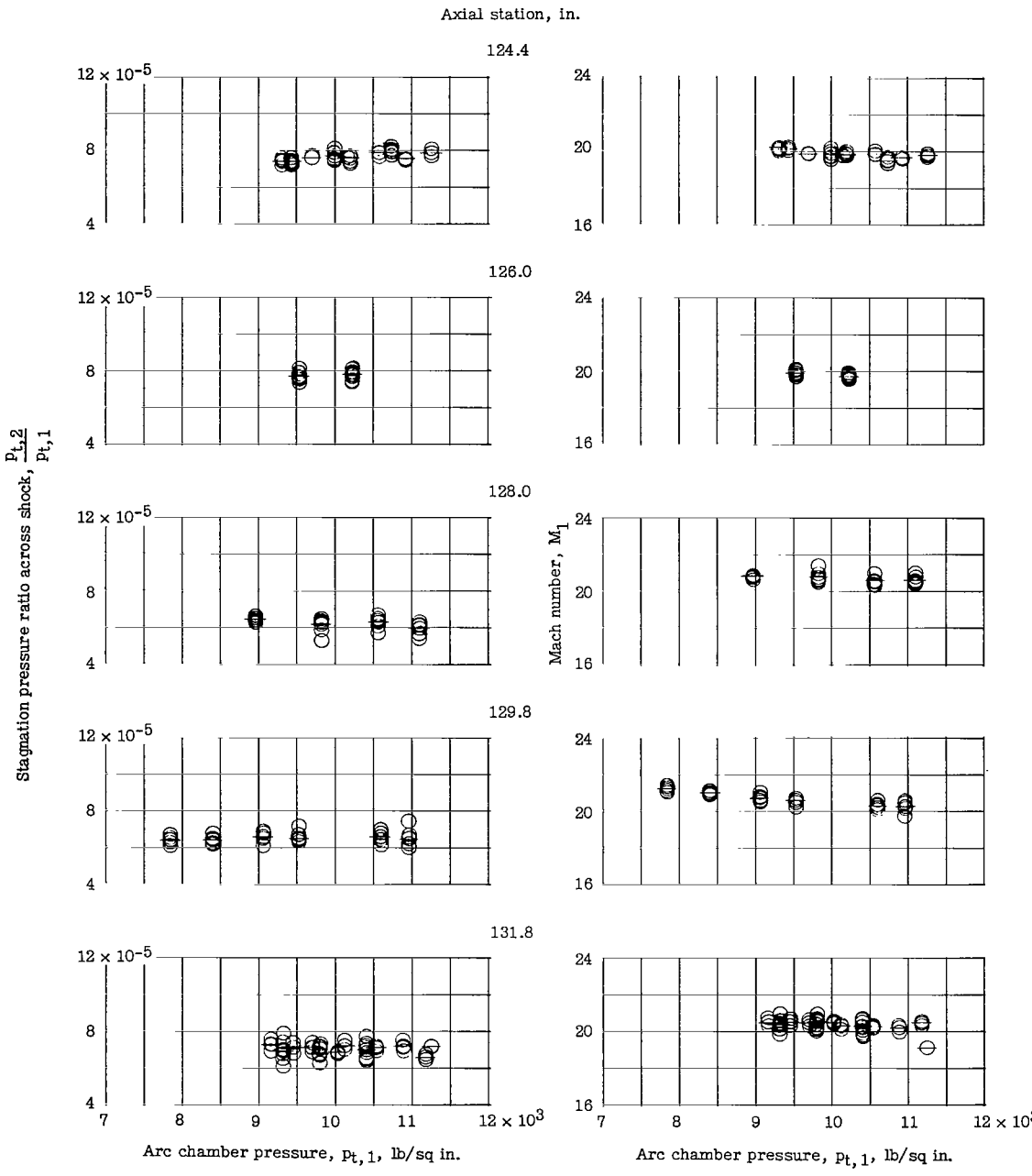

(a) Horizontal survey.

Figure 15.- Variation of stagnation pressure ratio and Mach number within the usable 8-inch-diameter test core with arc-chamber pressure. (The horizontal dashes represent the average of the plotted values for a particular $p_{t,1}$ to be used in subsequent plots; run time = 10 to 30 msec.)

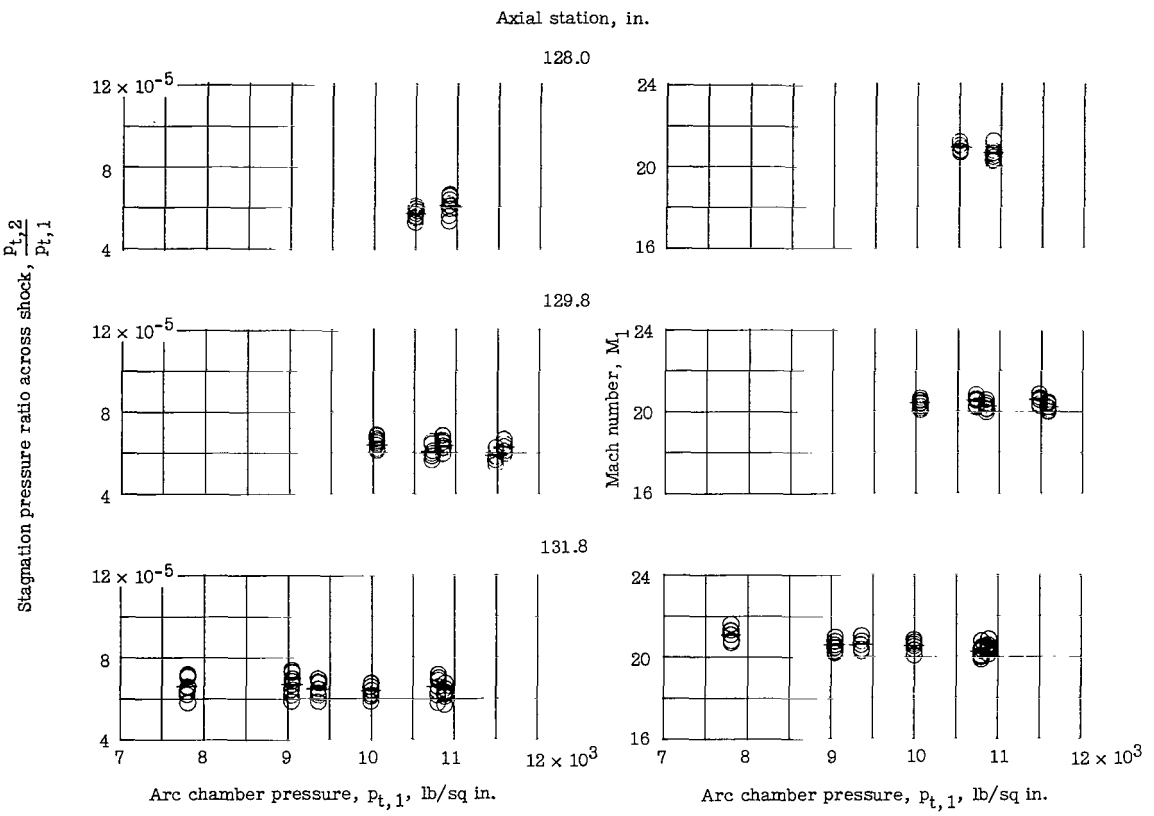

(b) Vertical survey.

Figure 15.- Concluded.

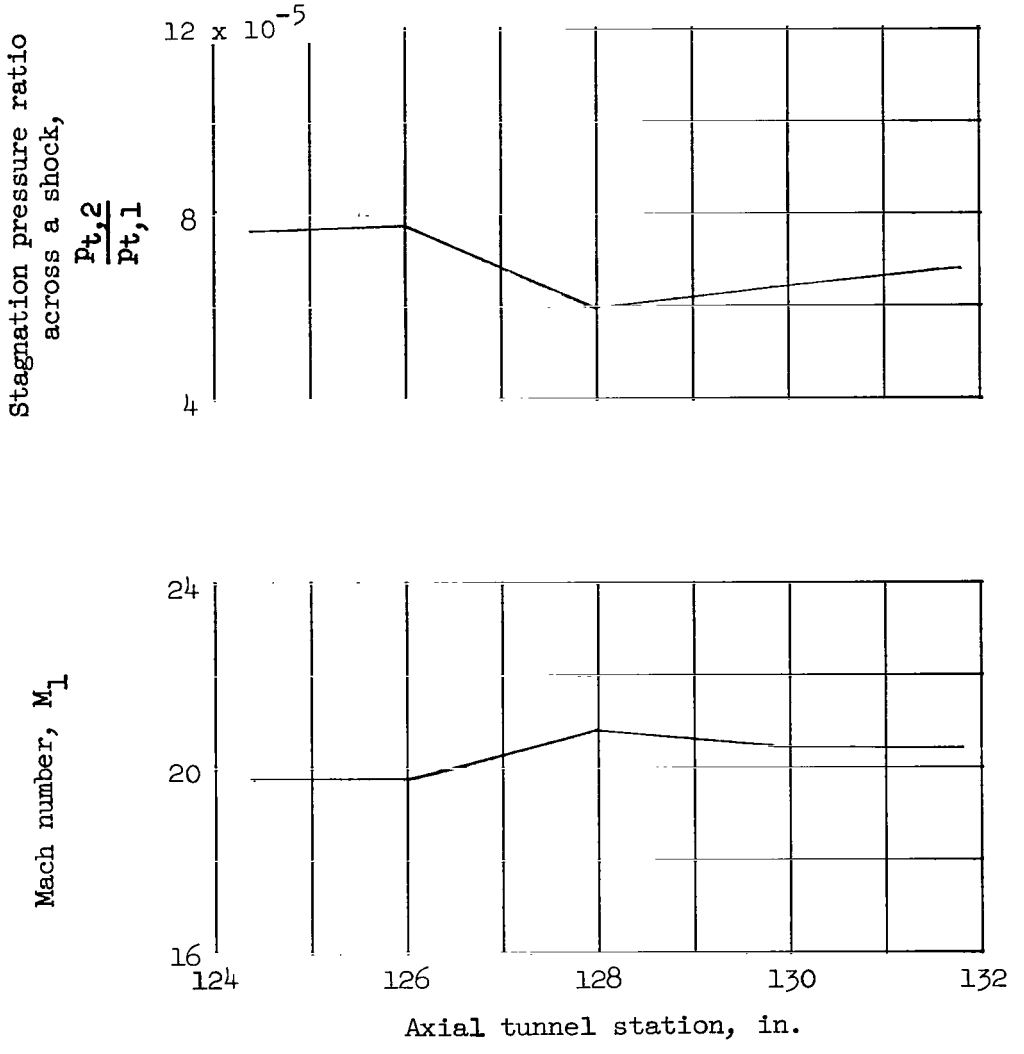

Figure 16.- Axial variation of the average stagnation pressure ratio and Mach number within the usable 8-inch-diameter test core.

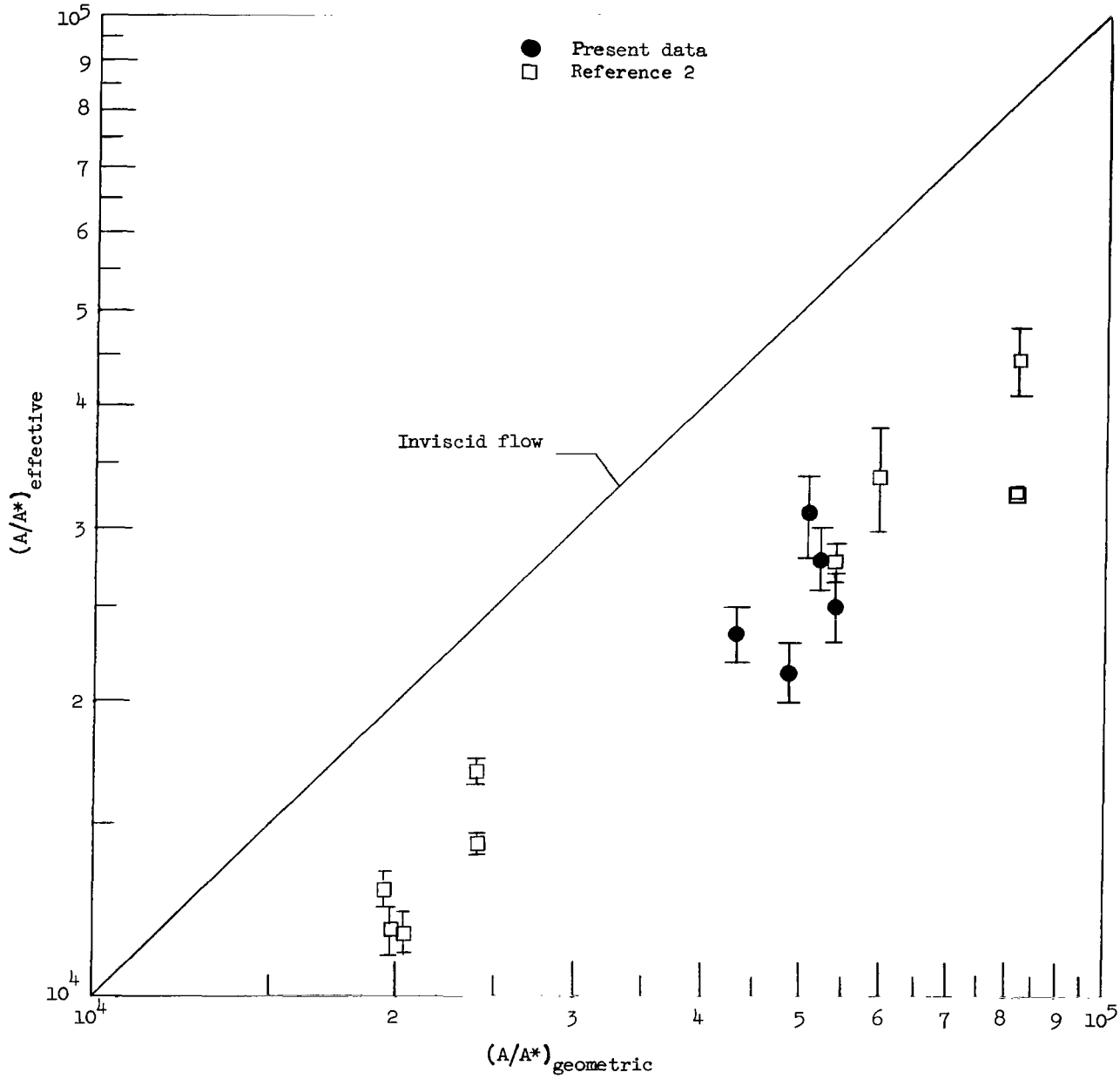

Figure 17.- Variation of the effective area ratio with geometric area ratio of the nozzle.

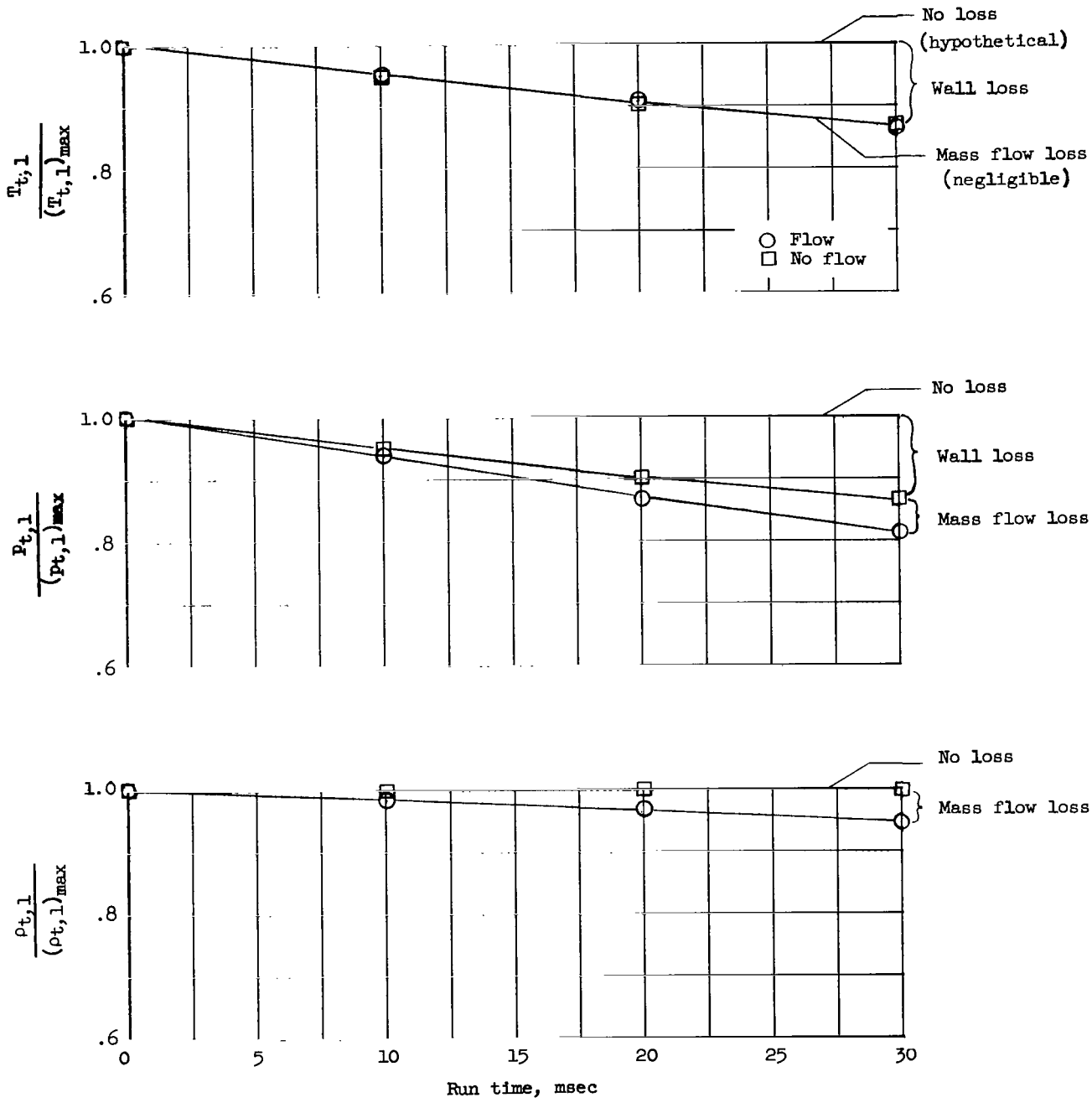

Figure 18.- Decay of arc-chamber conditions for shots with and without nozzle flow. $(T_{t,1})_{max} \approx 3400^{\circ}$ K; $(p_{t,1})_{max} \approx 12,300$ lb/sq in.; $(\rho_{t,1})_{max} \approx 62$ amagat.

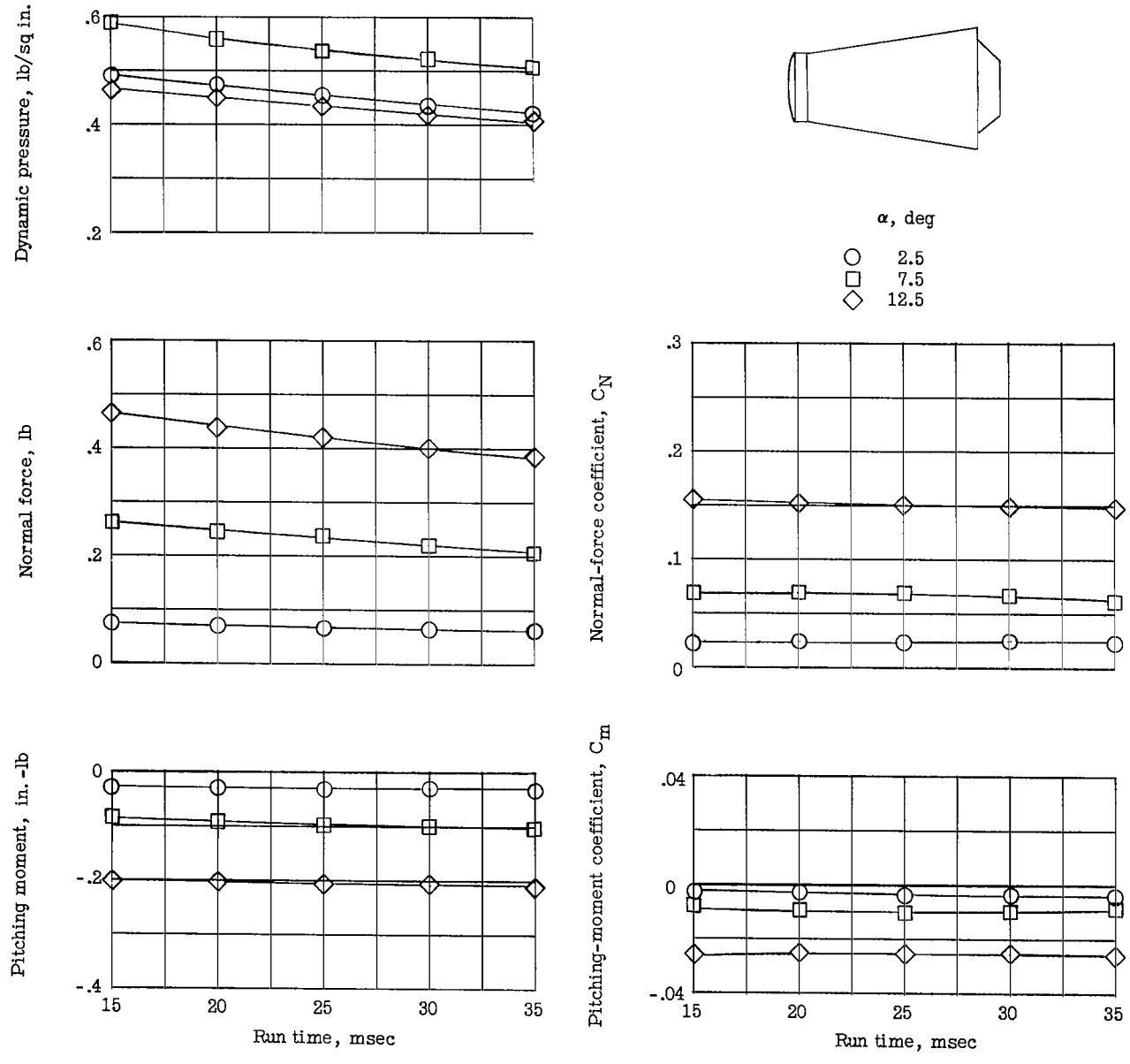

Figure 19.- Variation of representative strain-gage balance data in the Langley hotshot tunnel with run time for a Mach number of 20.

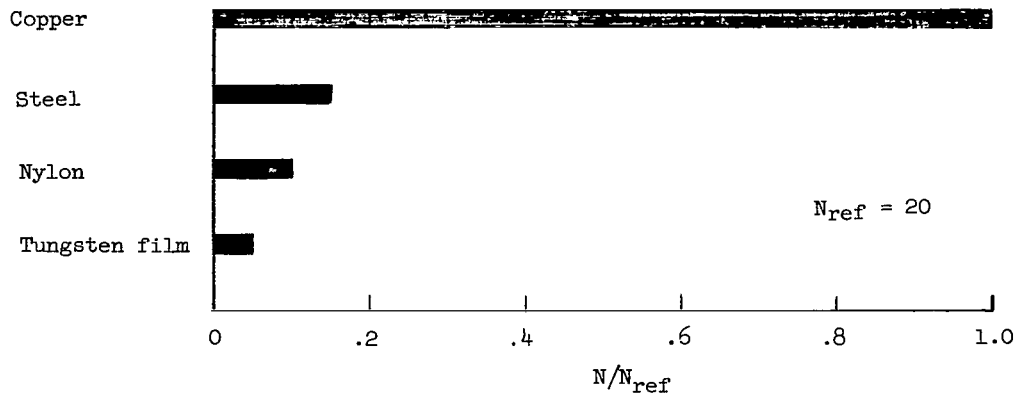

(a) Liner.

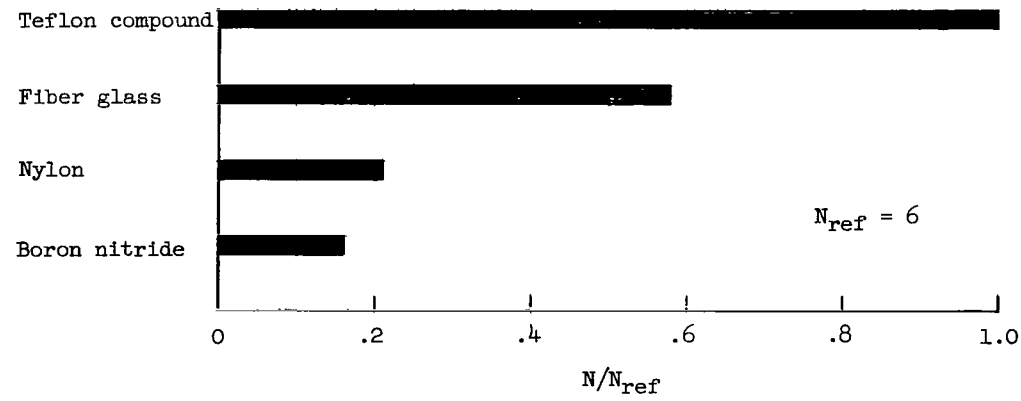

(b) Insulator components.

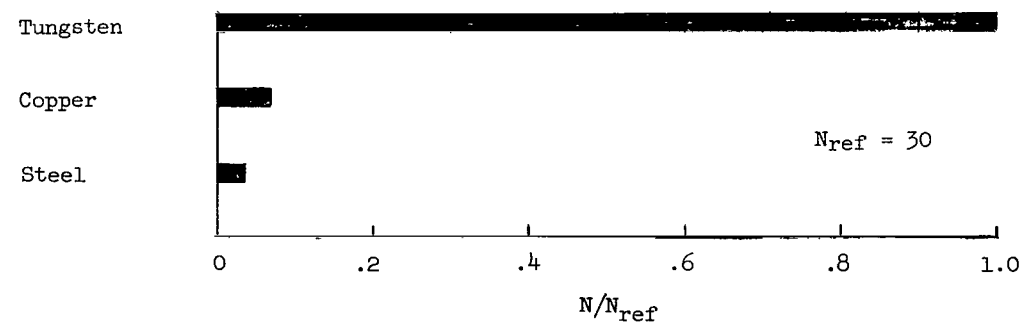

(c) Throat.

Figure 20.- Usable life of arc-chamber components. ($T_{t,1}$ = 2250° to 3250° K; $p_{t,1}$ = 7600 to 11,600 lb/sq in.)

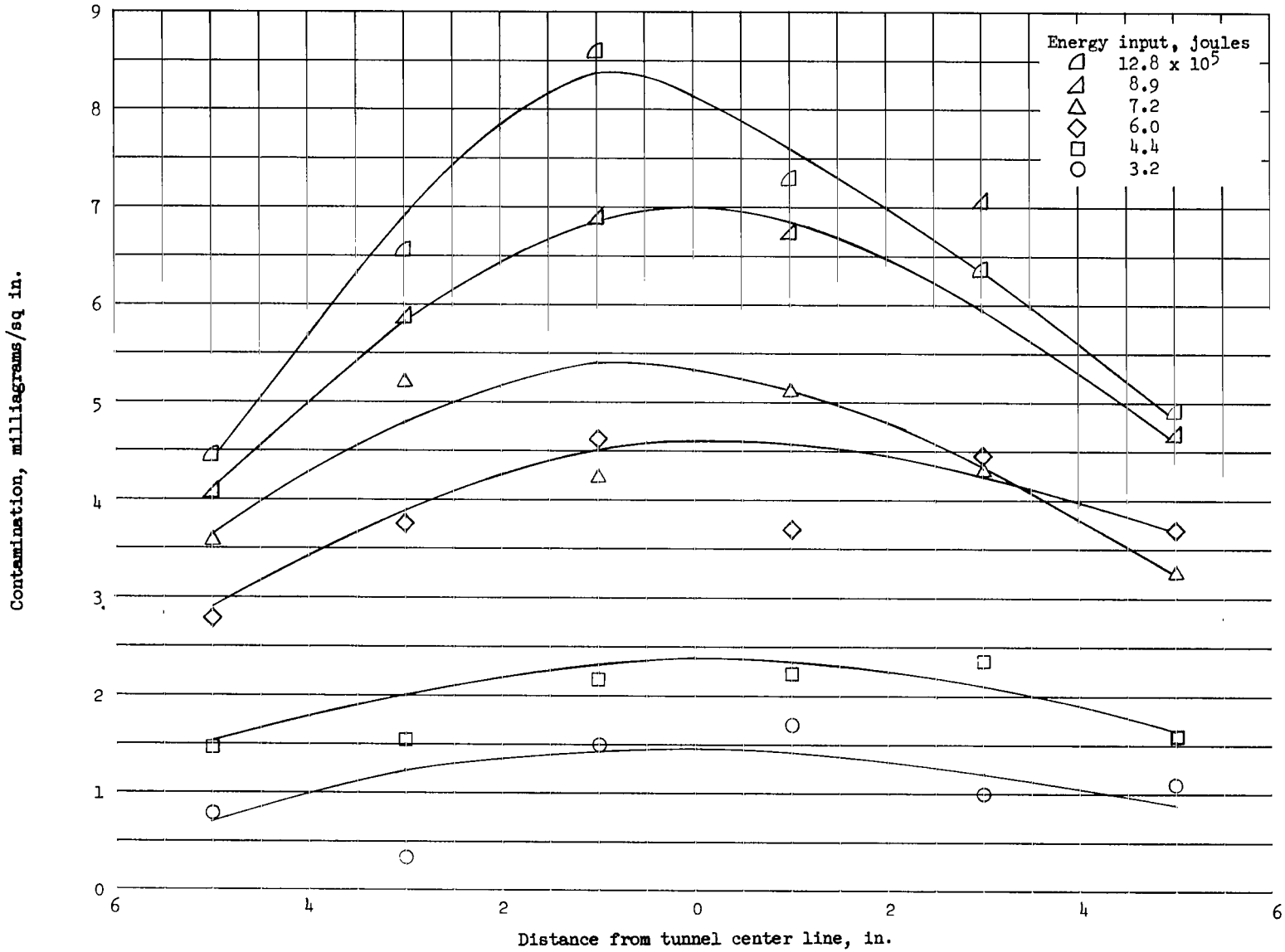

Figure 21.- Solid contamination results in the Langley hotshot tunnel.

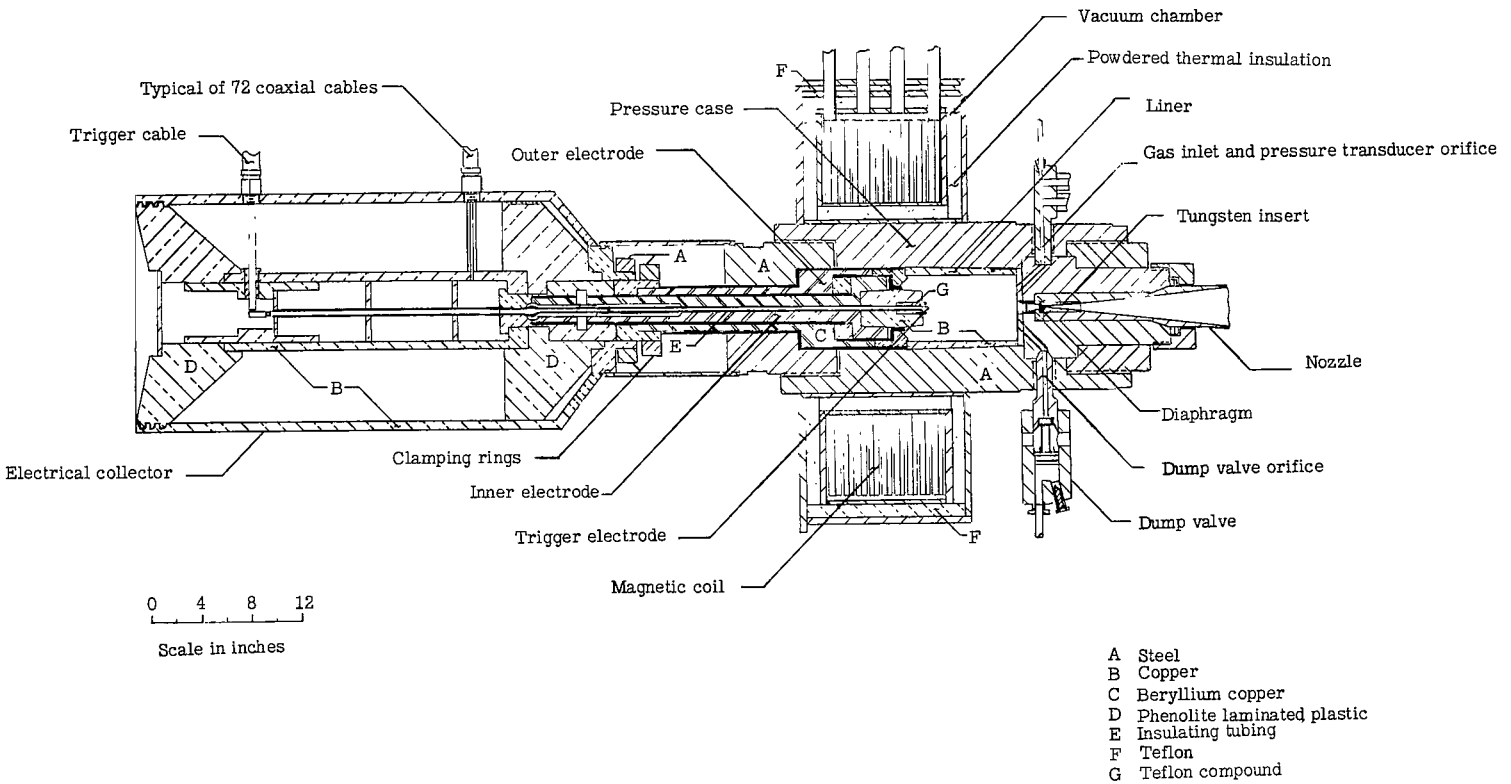

Figure 22.- Arc chamber for the Langley hotshot tunnel with end-firing coaxial electrodes.

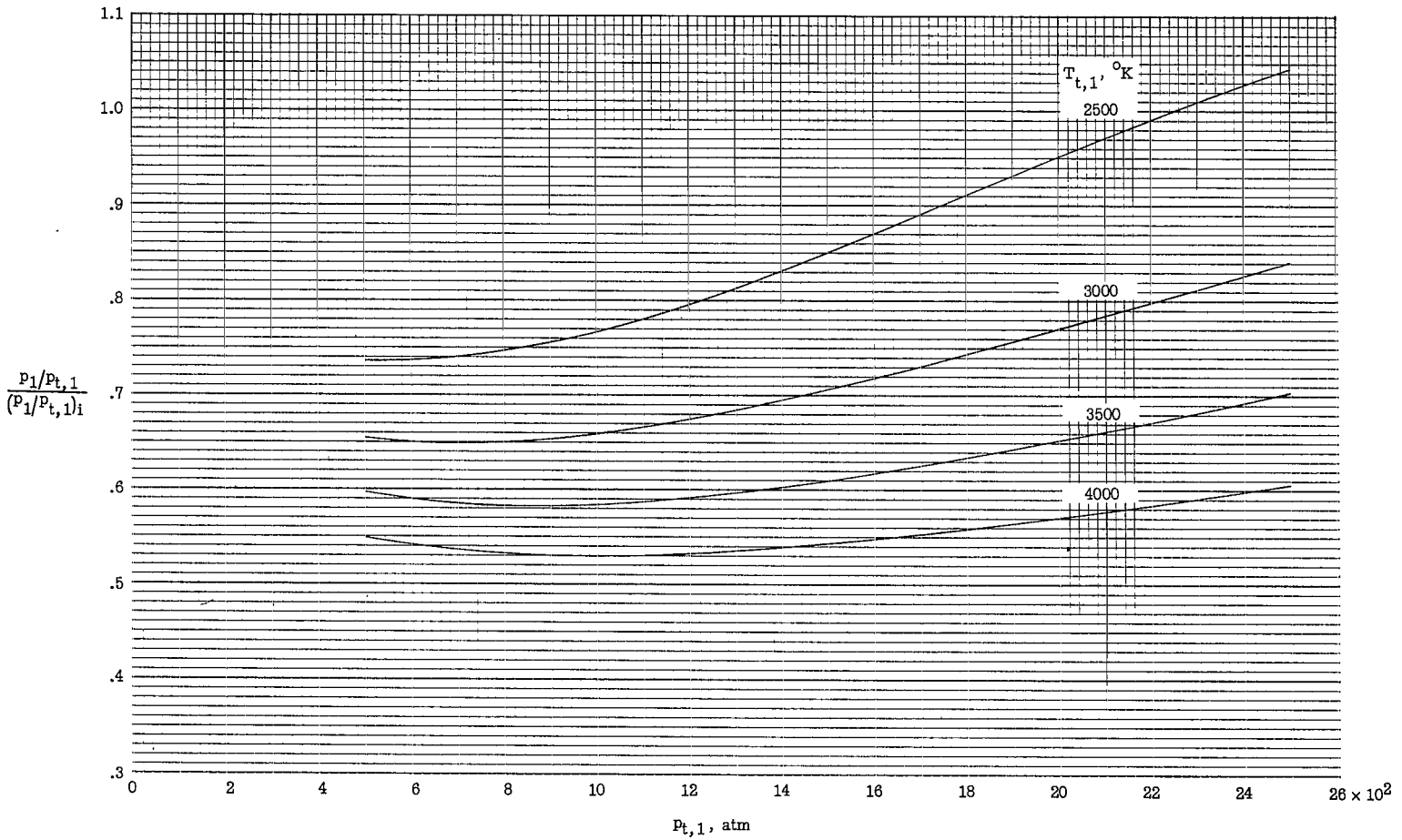

(a) $p_1/p_{t,1}$.

Figure 23.- Variation of ratios of real- to ideal-gas flow parameters with stagnation pressure for various stagnation temperatures where Mach number is greater than 10.

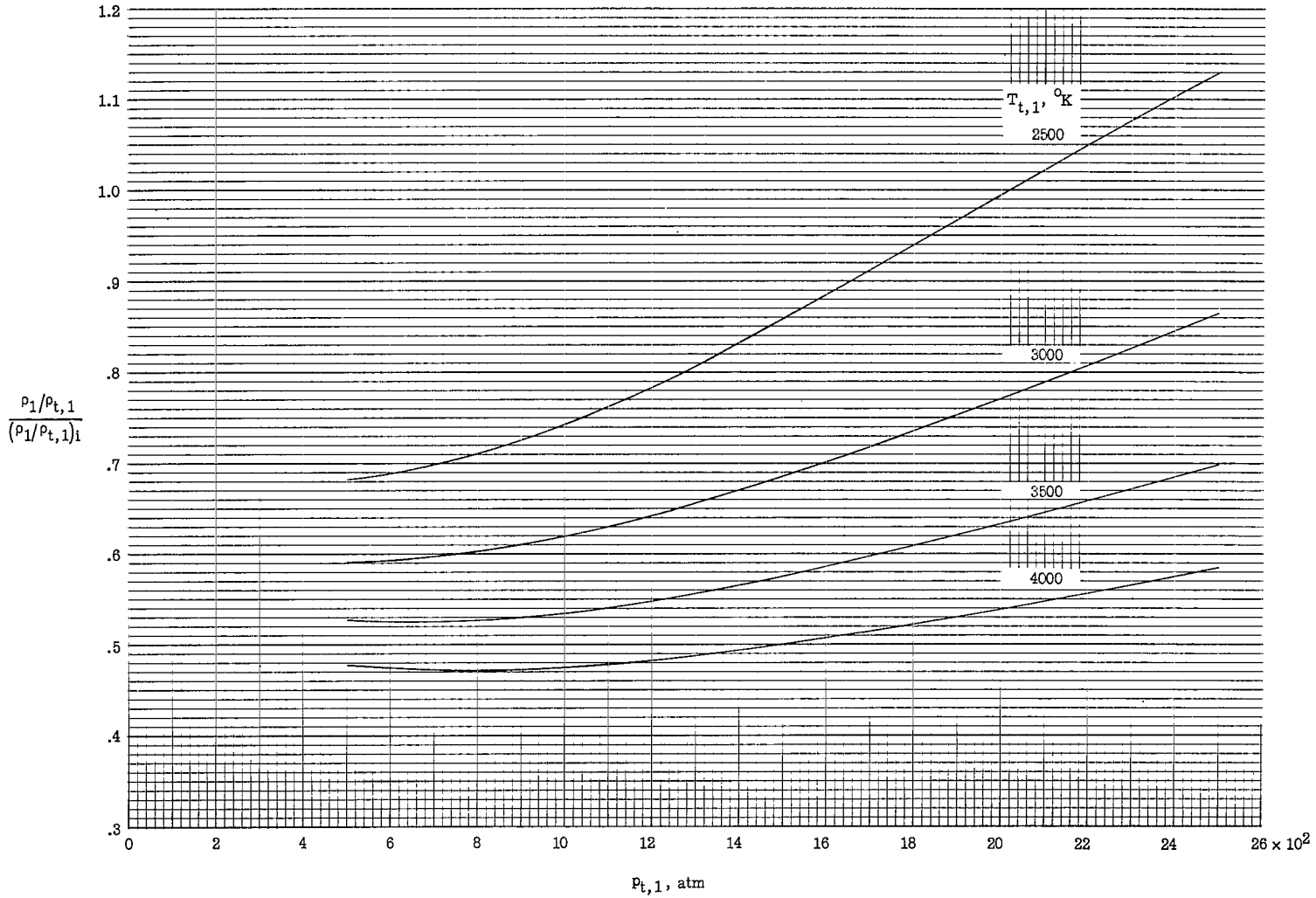

(b) $\rho_1/\rho_{t,1}$.

Figure 23.- Continued.

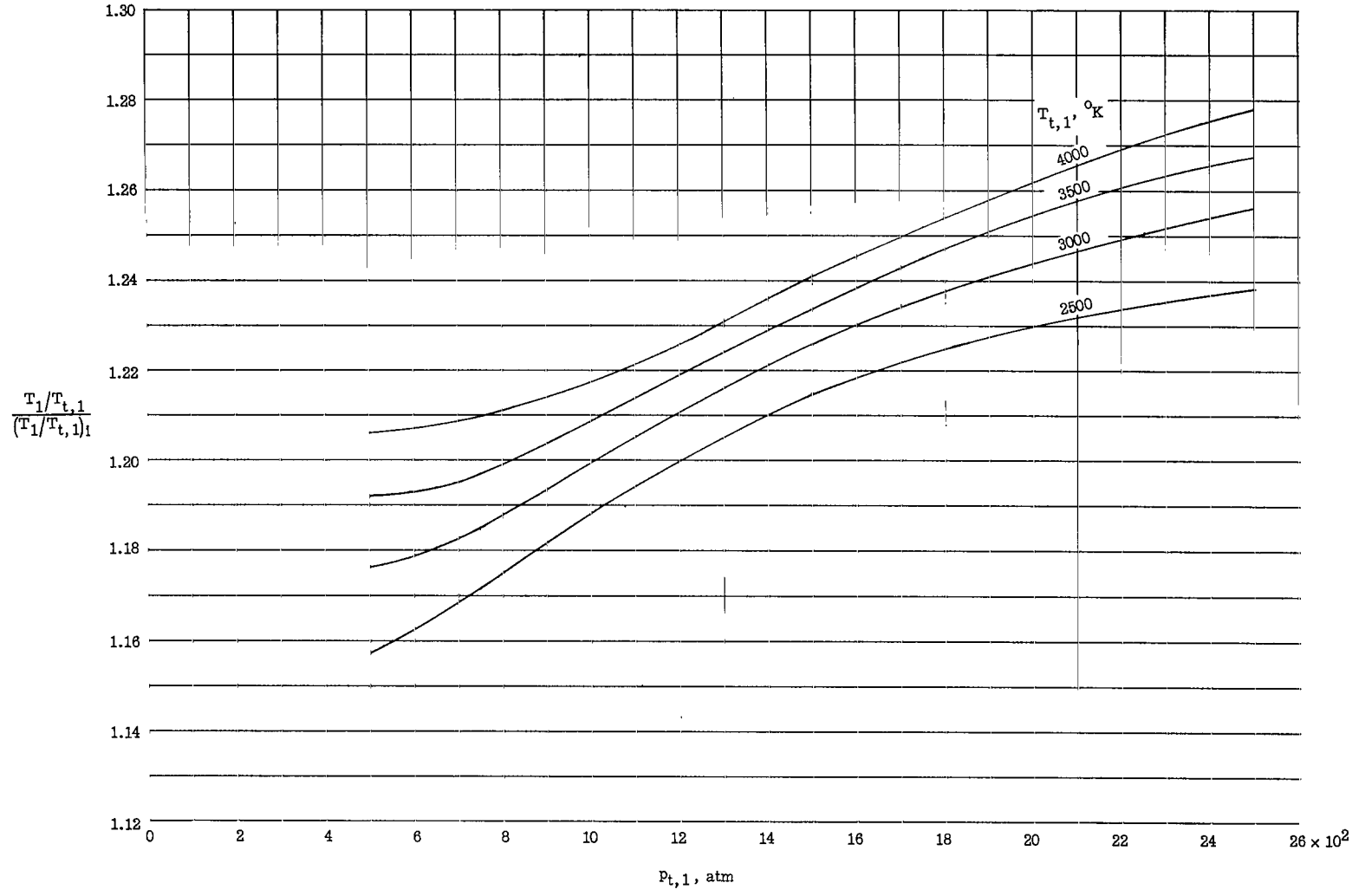

(c) $T_1/T_{t,1}$.

Figure 23.- Continued.

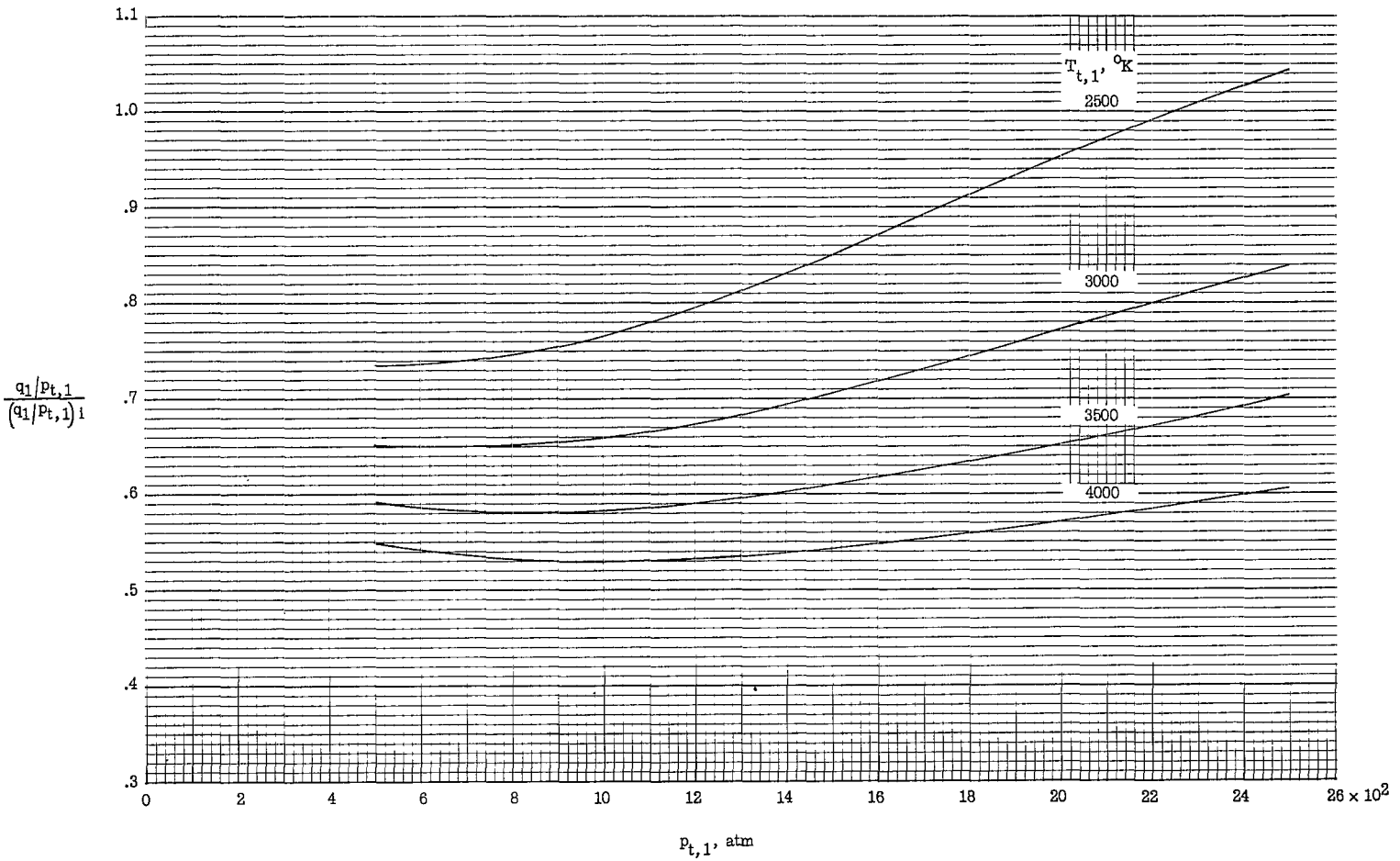

(d) $q_1/p_{t,1}$.

Figure 23.- Continued.

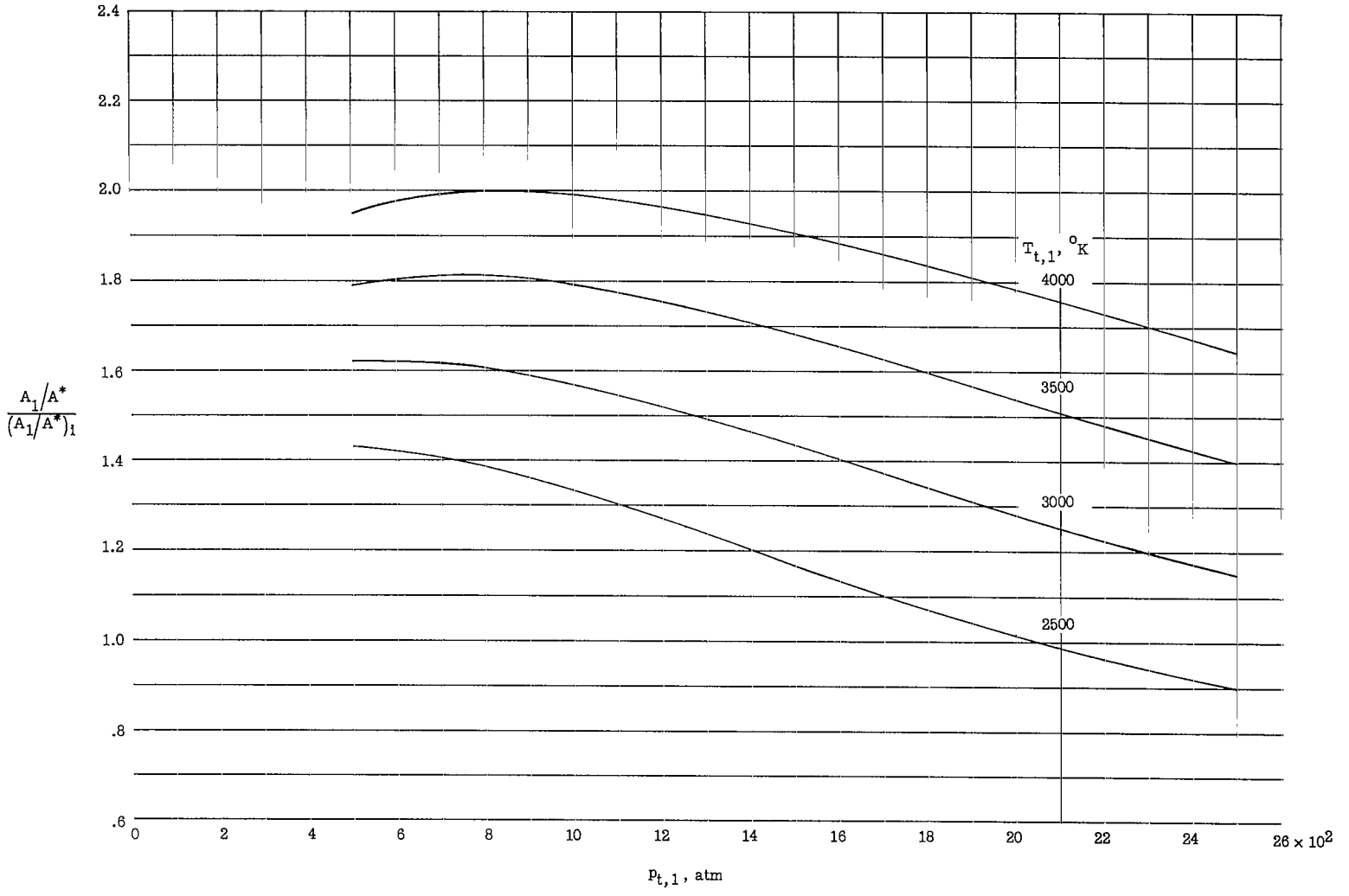

(e) A_1/A^*.

Figure 23.- Continued.

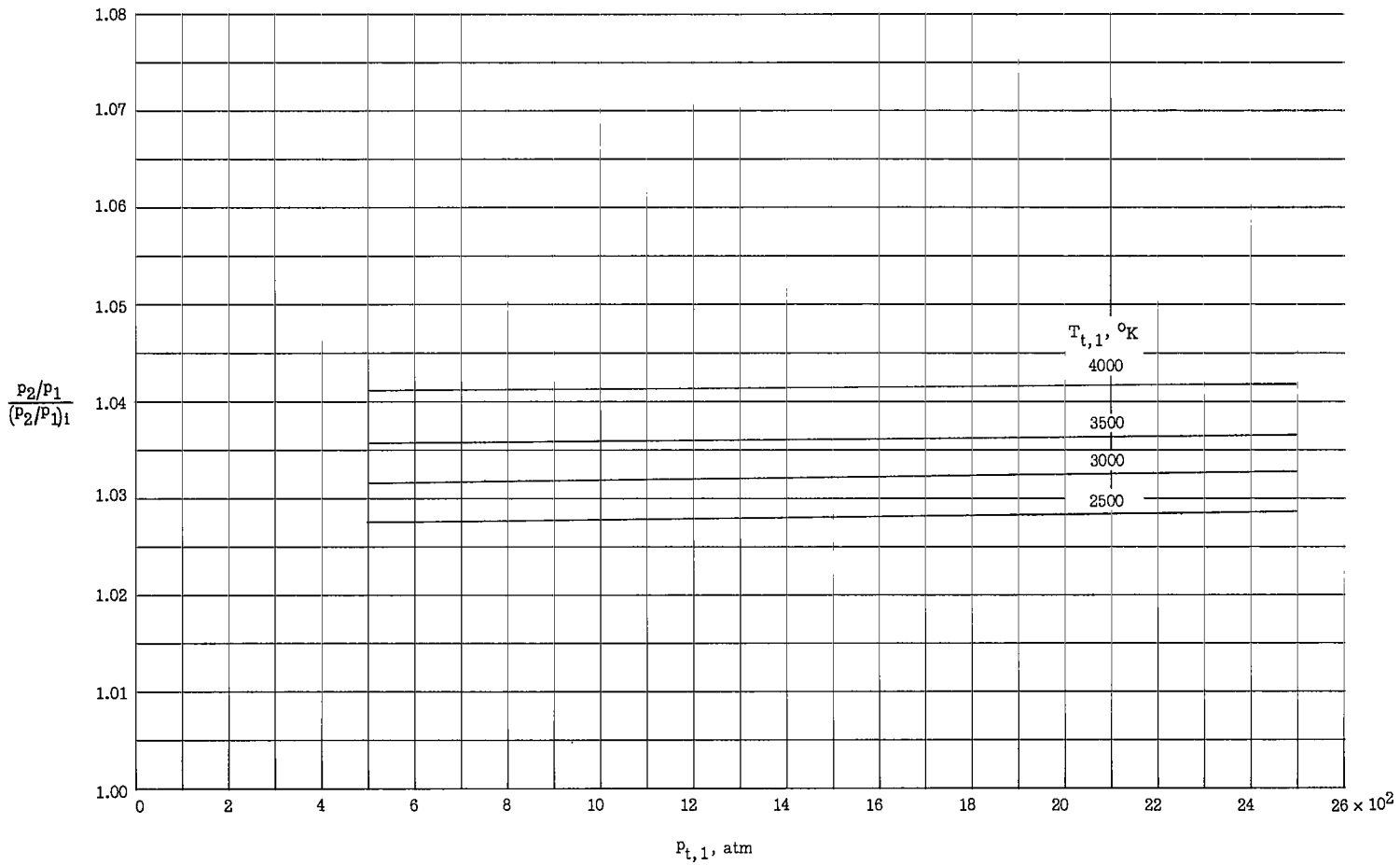

(f) p_2/p_1.

Figure 23.- Continued.

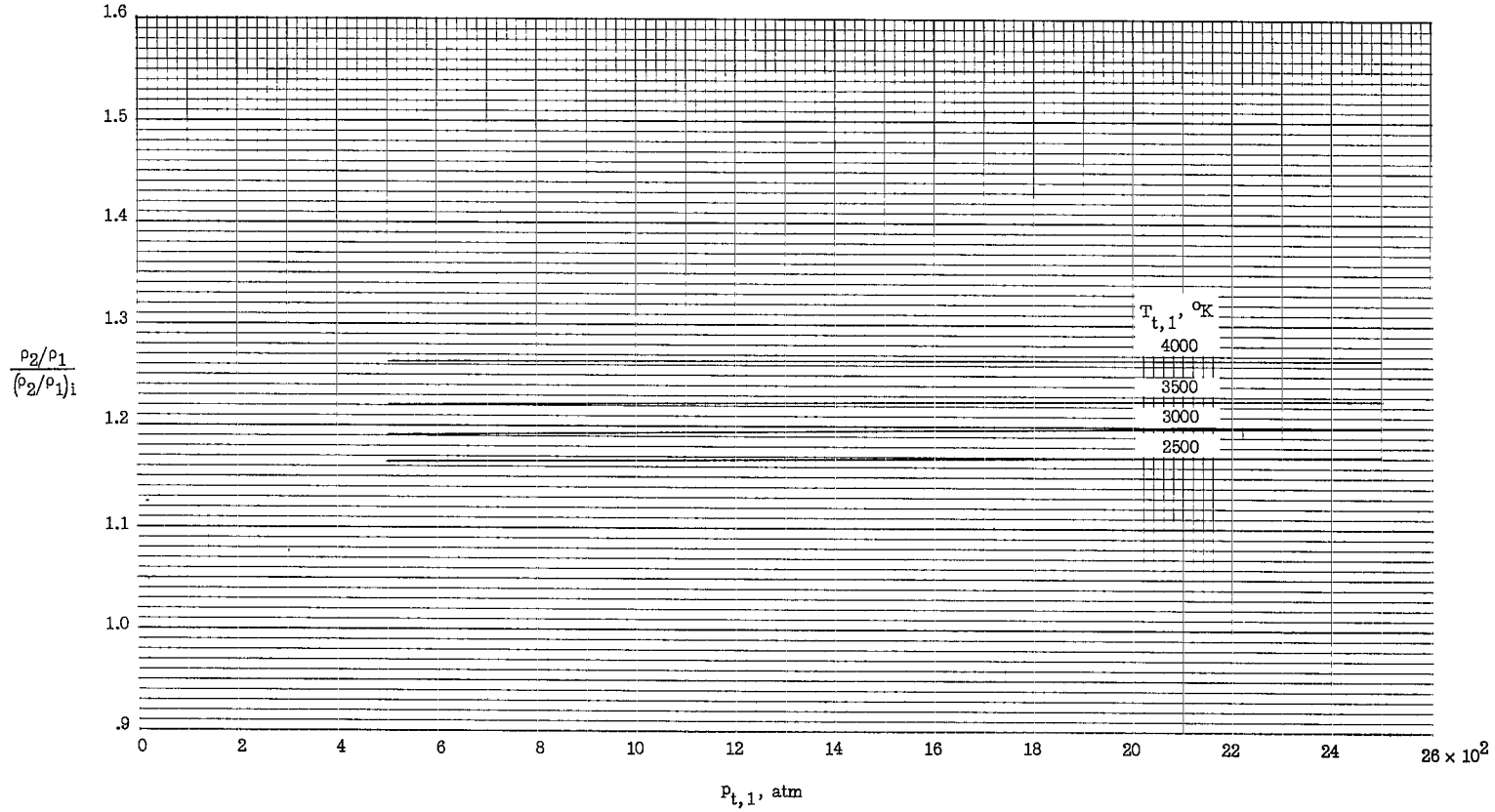

(g) ρ_2/ρ_1.

Figure 23.- Continued.

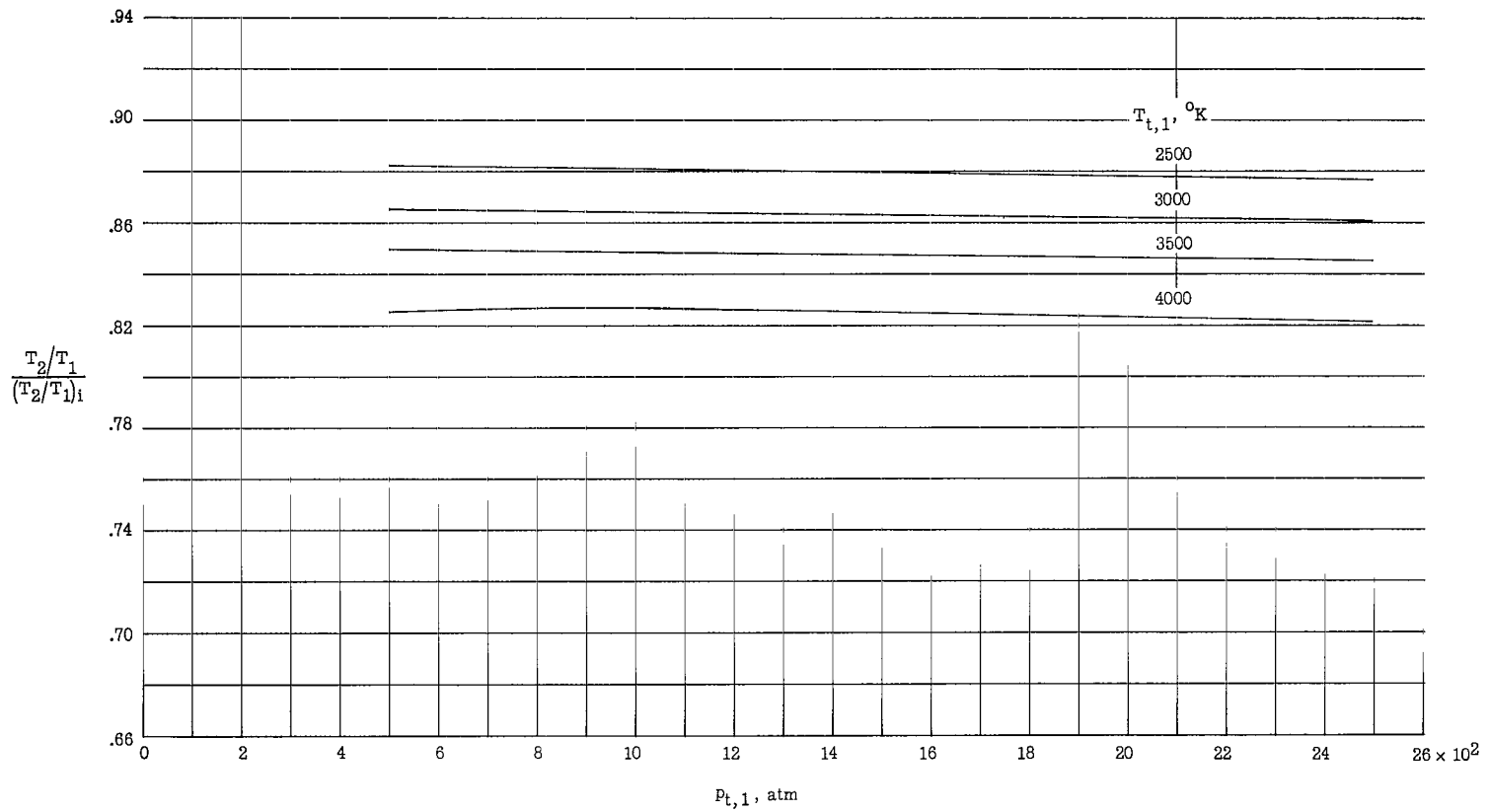

(h) T_2/T_1.

Figure 23.- Continued.

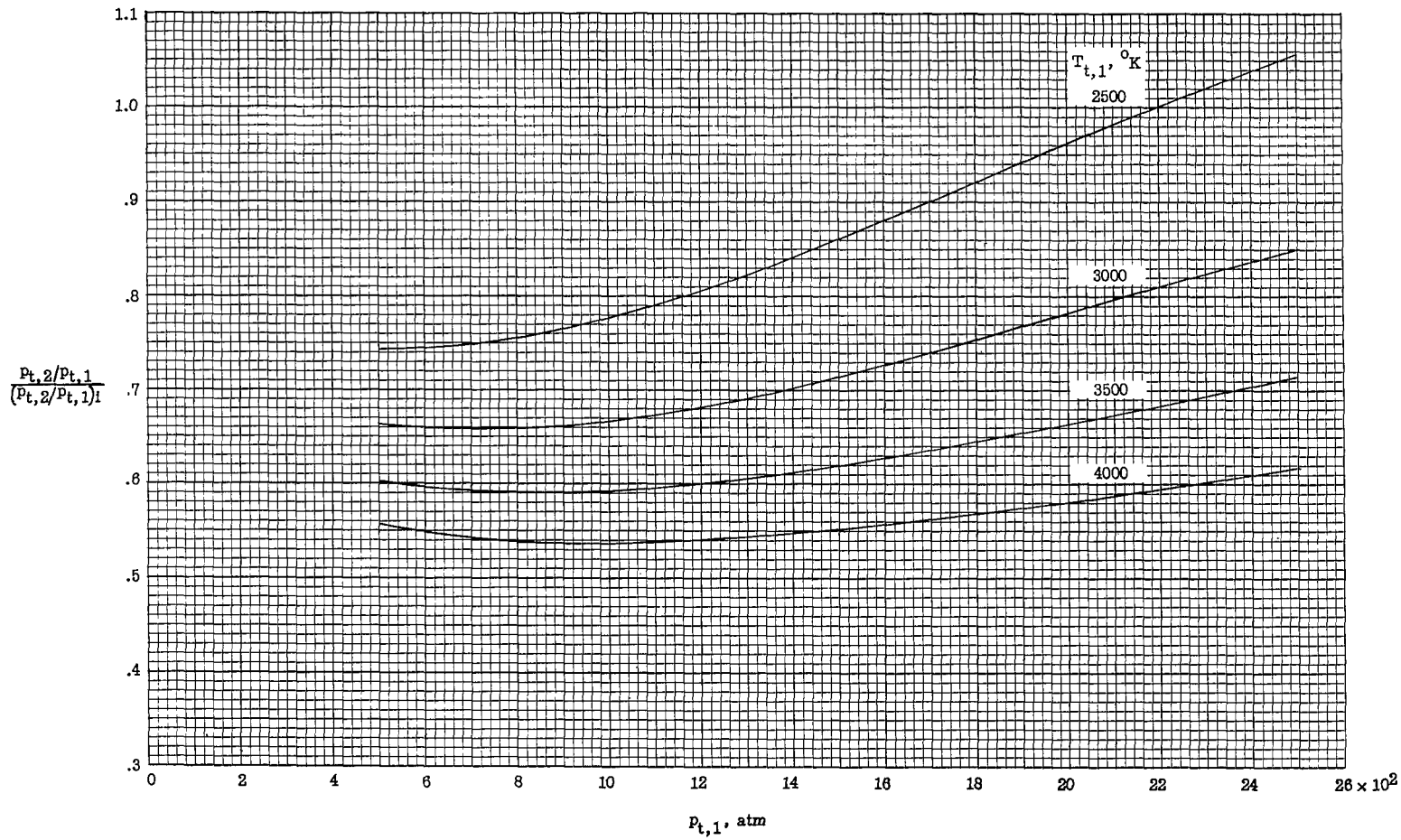

(i) $p_{t,2}/p_{t,1}$.

Figure 23.- Continued.

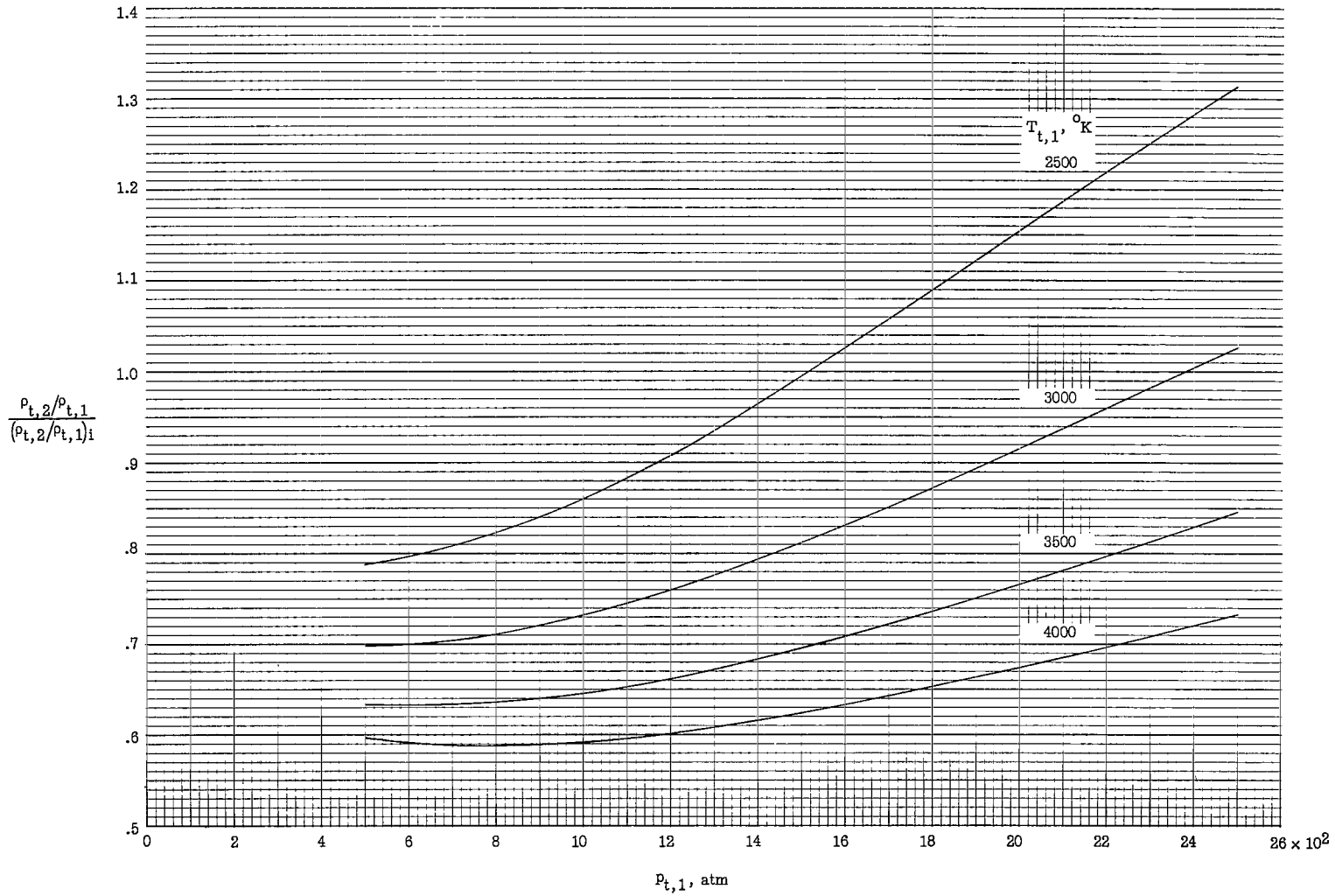

(j) $\rho_{t,2}/\rho_{t,1}$.

Figure 23.- Continued.

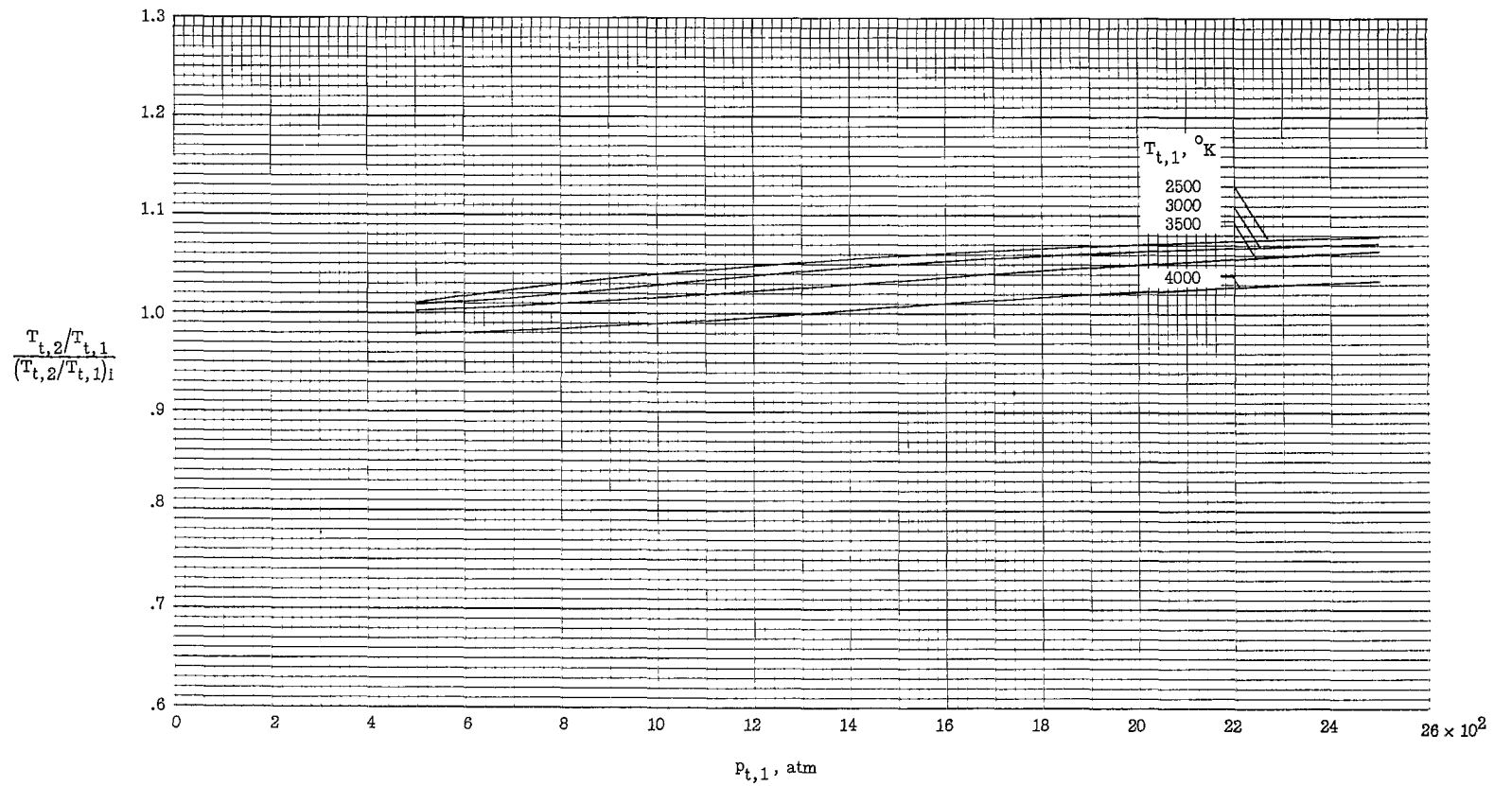

(k) $T_{t,2}/T_{t,1}$.

Figure 23.- Concluded.

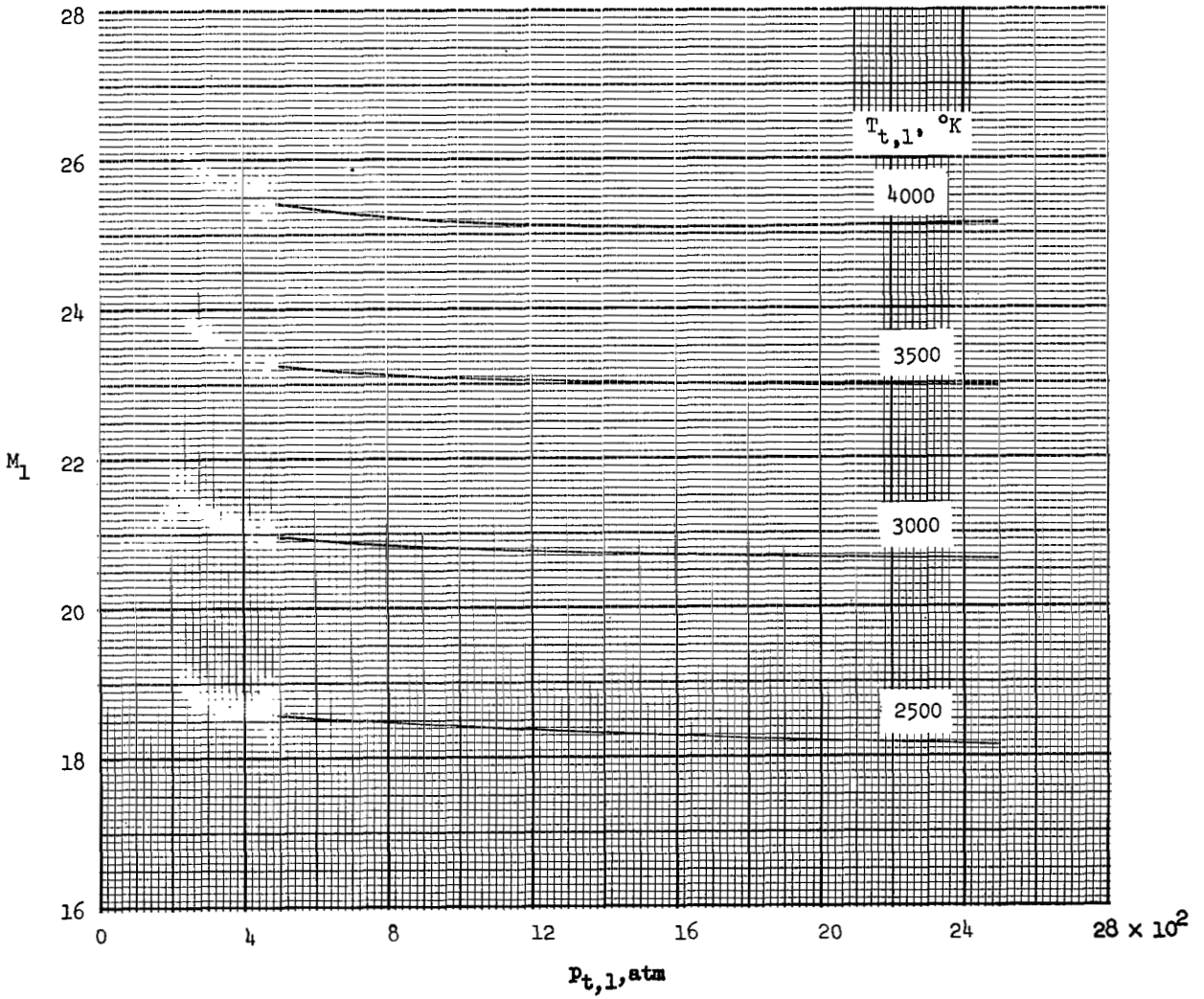

Figure 24.- Approximate maximum Mach number attainable without condensation for various reservoir stagnation pressures and temperatures.